Geochemistry Geophysics Geosystems G3
AN ELECTRONIC JOURNAL OF THE EARTH SCIENCES
Published by AGU and the Geochemical Society

Article
Volume 9, Number 3
7 March 2008
Q03007, doi:10.1029/2007GC001583
ISSN: 1525-2027

Evidence from high-Ni olivines for a hybridized peridotite/pyroxenite source for orogenic andesites from the central Mexican Volcanic Belt

Susanne M. Straub and Alexandra B. LaGatta
Lamont Doherty Earth Observatory at the Columbia University, 61 Route 9W, Palisades, New York 10964, USA (smstraub@ldeo.columbia.edu)

Ana Lillian Martin-Del Pozzo
Instituto de Geofisica, Universidad Nacional Autónoma de México, Ciudad Universitaria, Mexico DF 04510, Mexico

Charles H. Langmuir
Department of Earth and Planetary Sciences, Harvard University, 20 Oxford Street, Cambridge, Massachusetts 02137, USA

[1] Subduction zone magmatism produces calc-alkaline andesite melts that combine the high SiO_2, Na_2O, and K_2O abundances of the differentiated continental crust with low FeO, FeO/MgO, and TiO_2 typical of melts from depleted mantle. Ni-rich olivines in basaltic andesites and andesites of the central Mexican Volcanic Belt suggest that this dichotomy reflects a particular mechanism of mantle processing in the subduction environment. Hydrous slab components rich in Si, Na, and fluid mobile large-ion lithophile elements (LILE) transform mantle olivine to "reaction orthopyroxene." Along the ascent paths, and embedded into surrounding peridotite, secondary pyroxenite lithologies are created that are composed of "reaction orthopyroxene" next to mantle clinopyroxene and orthopyroxene. Partial melts from peridotite and pyroxenite then mix to produce primary calc-alkaline basaltic andesites and andesites that are rich in Na and LILE. The steady slab flux maintains high levels of Na and LILE in the mantle source but also induces repetitive melting that steadily depletes the subarc mantle in FeO, TiO_2, and other high field strength elements. If mantle processing thus creates primary basaltic andesite and andesite melts with the fractionated major element signature of the continental crust, the high magnesium number (Mg # (=Mg/Mg + Fe^{2+})) ~60–70 of these melts still requires additional differentiation to arrive at the lower Mg # ~55 of average continental crust.

Components: 54,284 words, 17 figures, 9 tables.

Keywords: Mexican Volcanic Belt; Ni-rich olivine; andesite genesis.

Index Terms: 1031 Geochemistry: Subduction zone processes (3060, 3613, 8170, 8413); 1037 Geochemistry: Magma genesis and partial melting (3619); 1065 Geochemistry: Major and trace element geochemistry.

Received 13 January 2007; **Revised** 1 November 2007; **Accepted** 5 December 2007; **Published** 7 March 2008.

Straub, S. M., A. B. LaGatta, A. L. Martin-Del Pozzo, and C. H. Langmuir (2008), Evidence from high-Ni olivines for a hybridized peridotite/pyroxenite source for orogenic andesites from the central Mexican Volcanic Belt, *Geochem. Geophys. Geosyst.*, *9*, Q03007, doi:10.1029/2007GC001583.

1. Origin of Orogenic Andesites

[2] Orogenic andesites are characterized by high abundances of Si, Na, Al and fluid mobile large-ion lithophile elements (LILE) relative to depletions in Fe, heavy rare earth elements (REE), Ti and other high field strength elements (HFSE) [e.g., *Gill*, 1981; *Tatsumi and Eggins*, 1995]. Despite their importance for evolutionary models of the continental crust, which orogenic andesites strongly resemble [e.g., *Kelemen*, 1995; *Rudnick*, 1995], the cause of this dichotomy of enrichment versus depletion remains unresolved. In subduction settings, where andesitic melts prevail, the high ratio of LILE relative to HFSE and REE ratios have been linked to the processing of chemical components from multiple sources [e.g., *Chesley et al.*, 2002; *Gómez-Tuena et al.*, 2003; *Hildreth and Moorbath*, 1988; *Morris et al.*, 1990; *Pearce and Peate*, 1995; *Plank and Langmuir*, 1993; *Wörner et al.*, 1992]: (1) the subducting hydrated lithosphere composed of sediment (~400 m), basaltic crust (~6 km) and lithospheric mantle (several tens kilometers); (2) the convecting subarc mantle of ~50–120 km thickness at arc front depths, and (3) the upper plate crust of variable thickness (20–70 km) and composition on which the volcanic arcs are constructed. Major element compositions, however, are usually not considered in such models, even though they make up >99% of the melt mass and hence must have implications for melt origin and formation. Current models advocate the upper plate crust [e.g., *Davidson*, 1987; *Hildreth and Moorbath*, 1988; *Tamura and Tatsumi*, 2002; *Tatsumi*, 2000], the subarc mantle [*Kelemen*, 1995; *Kelemen et al.*, 2004; *Plank and Langmuir*, 1988] or the subducting slab [e.g., *Defant and Drummond*, 1990; *Kay*, 1978] as significant melt mass contributors. Each of these models emphasizes different processes of differentiation (e.g., melting, mixing, melt-rock reaction, assimilation, fractional crystallization) to create the broader spectrum of orogenic andesites. The crucial problem of this debate is that to date no chemical tracer has been identified that distinguishes among the sources for major element oxides. Here we present new Ni data in olivine phenocrysts from the central Mexican Volcanic Belt (MVB), a Quaternary volcanic arc that is constructed on thick continental crust. We infer that the unusually high Ni of the olivines constrains the formation of primary basaltic andesite and andesite melts from a subarc mantle that has been partially transformed to pyroxenite mantle by reaction with components from slab. Since similar Ni-rich olivines have been reported from other arcs, e.g., the Cascades [*Clynne and Borg*, 1997], Japan [*Tatsumi et al.*, 2006], the Aleutians and Kamchatka arcs (P. Kelemen, personal communication, 2007), the model proposed has broader significance.

2. Geological Setting: Central Mexican Volcanic Belt

[3] The central Quaternary Mexican Volcanic Belt (MVB) (Figure 1, between 100° and 98°30′W) is constructed on 40–47 km thick sialic crust of the Grenvillian (Proterozoic) Oaxaquaia microcontinent (see *Gómez-Tuena et al.* [2006] for review). Within a 30 km wide segment of only ~70 km length along strike of the arc, a broad spectrum of alkaline and calc-alkaline basaltic to dacitic melts has erupted within the last few 100 ka (Figure 2 and Table 1). The central MVB series form a continuum in compositional space between two end-members (Figures 2–4) [*LaGatta*, 2003; *Schaaf et al.*, 2005; *Wallace and Carmichael*, 1999]. No clear boundaries exist, but for the purpose of presentation and discussion, it is useful to define three groups [*LaGatta*, 2003]. The "calc-alkaline end-member group" refers exclusively to the calc-alkaline magnesian andesites and dacites of the composite stratovolcanoes, such as Popocatepetl (Popo) or Nevado de Toluca (=Toluca). These magmas have low FeO* and HFSE abundances, low FeO*/MgO ratios at high SiO_2, but the highest LILE abundances and high LILE/REE and LILE/HFSE ratios (e.g., Ce/Pb ~ 4, Ba/La ~ 26, Li/Nb ~ 3.9) (Figures 2 and 3). The second end-member group ("alkaline group") are mildly alkaline basalts and basaltic andesites (also "OIB-type" series [*Gómez-Tuena et al.*, 2006]) that erupt from monogenetic volcanoes located equidistant to Popo and Toluca in the central Sierra Chichinautzin Volcanic Field (SCVF) (Figure 1) [*LaGatta*, 2003]. Alkaline volcanics have the highest FeO* and HFSE abundances (Nb > 20–34 ppm) of the central MVB series but only moderate relative enrichments of some of the highly fluid mobile LILE (e.g., Cs, B, Pb; Figures 2 and 3). Their enriched trace element patterns are comparable to the Quaternary alkaline basalts of the Mexican Basin and Range Province (Basin and Range basalts). The Basin and Range basalts erupt behind the arc front and likely represent melts from the mantle beneath the North American Plate prior to subduction modification (Figures 2 and 3) [*Gómez-Tuena et al.*, 2003, 2006; *Luhr*, 1997; *Luhr et al.*,

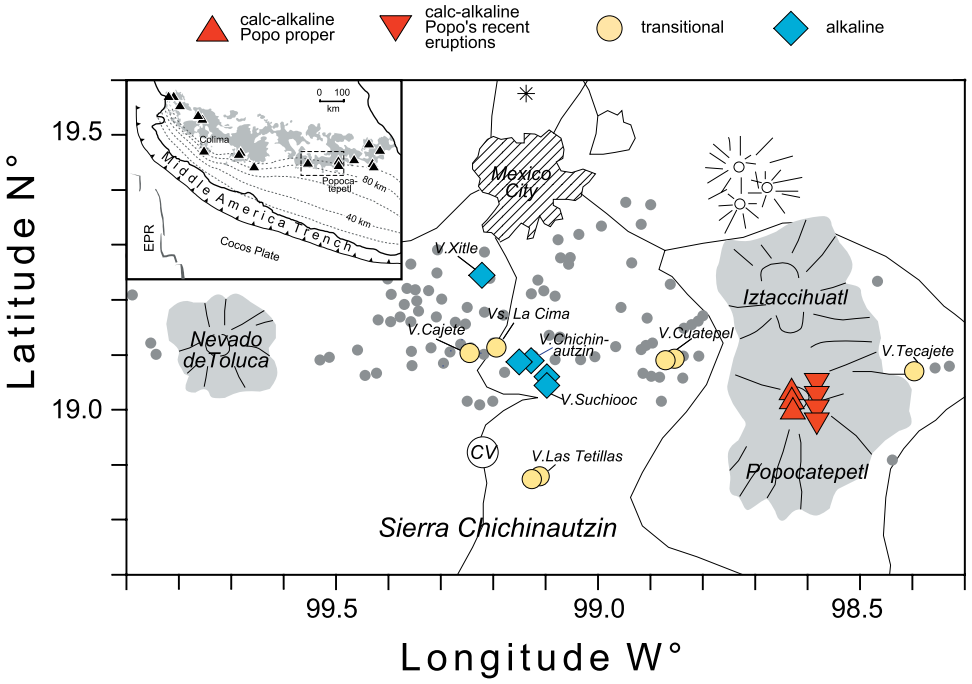

Figure 1. Study area in the central Mexican Volcanic Belt (MVB) south of Mexico City. The central MVB is located ~100 km above the nearly horizontally subducting Cocos Plate. Quaternary composite volcanoes Popocatepetl/Iztaccihuatl and Nevado de Toluca flank the monogenetic Sierra Chichinautzin Volcanic Field (SCVF) with >200 monogenetic volcanoes. Colored symbols are sample locations of calc-alkaline (normal and inverted red triangles), transitional (yellow circles), and alkaline groups (blue diamonds). See text for definition of compositional groups. EPR is East Pacific Rise.

1989, 1995b, 1995a; *Pier et al.*, 1989; *Wallace and Carmichael*, 1999]. The third "transitional group" summarizes the remaining series with an arbitrarily chosen Nb < 20 ppm from the monogenetic centers of the Sierra Chichinautzin. These include calk-alkaline basalts to dacites as well as compositions that trend toward the alkaline group (Figures 2 and 3).

[4] Given the limited age range (a few hundred kiloannum [*Schaaf et al.*, 2005; *Siebe et al.*, 2004b]), and the constant subduction parameters of the central MVB series investigated (e.g., crustal thickness, slab composition, convergence rate, height above slab etc.), the compositional diversity of the central MVB must reflect either differentiation processes, or source heterogeneity. The presence of alkaline basalts, that cannot originate from the continental crust, implies that mantle melts may pass through the thick crustal basement nearly unchanged. The origin of the calc-alkaline melts, however, is more ambiguous. Primitive calc-alkaline basalts to andesites have high magnesium numbers (Mg # (=g/Mg + Fe^{2+})) (~70) and Ni (~100–250 ppm) and Cr (~200–500 ppm) abundances which are close to those of primary mantle melts [*Blatter and Carmichael*, 1998b, 2001; *Straub and Martin-Del Pozzo*, 2001]. However, no consensus exists as to whether primitive calc-alkaline melts may be (1) near-primary mantle melts [e.g., *Blatter and Carmichael*, 1998b; *Carmichael*, 2002; *Kelemen*, 1995; *Wallace and Carmichael*, 1999], (2) slab melts that were further modified in the mantle [e.g., *Gómez-Tuena et al.*, 2007; *Martinez-Serrano et al.*, 2004; *Rapp et al.*, 1999], or (3) melts that already have been significantly modified the upper plate crust by fractional crystallization and crustal assimilation/contamination [e.g., *Hildreth and Moorbath*, 1988; *Nixon*, 1988b; *Schaaf et al.*, 2005; *Siebe et al.*, 2004a; *Wallace and Carmichael*, 1999].

[5] Notably, the comprehensive set of high-quality trace element data and Sr-Nd-Pb-Hf isotopes ratios that are now available on these series remains inconclusive with respect to melt provenance [*Cai et al.*, 2007; *LaGatta*, 2003; *Schaaf et al.*, 2005; *Siebe et al.*, 2004a]. For example, there is no evidence for a garnet signature that would support a slab melt origin, or lower crustal melt. The (Tb/

Table 1. Major and Trace Element Composition of Bulk Rock[a]

	Alkaline Group					Transitional Group							Calc-alkaline Group									
	V Chichinautzin		V Suchiooc		V Xitle	V Cuatepel		Vs La Cima	Las Tetillas		C Tecajete	V Cajete	Popocatepetl Proper			Popocateptl's Recent Eruptions Series (Since 1994)				Repeat Analyses of Samples ASC1_S[c]		
	ASC1_S	ASC1_A	ASC44	ASC44B	SX25	SPO60	SPO56	LaCima3	LT4	LT3	SPO58B	SCEN22	TP6	SPO38	TP10C	30 April 1996	30 December 1996	30 June 1997	22 January 2001		SD	RSD, %
Latitude N	19°01′06″	19°01′06″	18°59′10″	18°59′10″	19°14′45″	19°05′13″	19°05′41″	19°06′39″	18°52′53″	18°52′53″	19°03′38″	19°06′10″	19°02′25″	19°03′47″	19°05′10″	19°01′25″	19°01′25″	19°01′25″	19°01′25″			
Longitude W	99°09′08″	99°09′08″	99°03′32″	99°03′32″	99°13′21″	98°51′46″	98°51′55″	99°11′58″	99°06′39″	99°06′39″	98°23′50″	99°14′29″	98°37′31″	98°40′31″	98°40′46″	98°37′21″	98°37′21″	98°37′21″	98°37′21″			
Analyst[b]	SMS	AL	AL	AL	AL	SMS	AL	SMS	SMS	SMS	AL	SMS	AL	AL	AL	SMS	SMS	SMS	SMS	SMS		
Major element, wt %																						
SiO2	52.8	53.3	51.2	51.2	52.0	58.9	55.6	52.7	53.2	53.3	54.9	51.0	62.9	59.5	59.0	63.2	64.5	58.7	59.0	52.8	0.3	0.7
TiO2	1.87	1.89	1.79	1.81	1.71	0.88	0.94	1.40	0.96	0.96	1.12	1.63	0.78	0.71	0.73	0.71	0.68	0.93	0.87	1.87	0.02	1.0
Al2O3	15.8	15.9	17.1	16.8	15.8	16.4	16.2	16.8	16.6	16.6	16.2	16.7	16.1	15.8	15.5	16.4	16.6	16.0	16.2	15.8	0.1	0.5
Fe2O3	9.58	9.60	9.32	9.41	9.16	6.25	7.05	8.98	8.12	8.10	7.31	9.25	5.25	5.80	5.85	5.02	4.57	6.51	6.22	9.58	0.02	0.2
MnO	0.16	0.16	0.14	0.15	0.13	0.10	0.11	0.14	0.13	0.13	0.11	0.14	0.09	0.10	0.1	0.08	0.08	0.11	0.10	0.16	0.00	1.0
MgO	5.91	5.76	7.24	7.13	7.67	5.40	7.04	7.55	7.98	8.15	6.85	7.53	3.36	5.60	6.86	3.90	2.62	6.73	5.58	5.91	0.04	0.7
CaO	6.95	6.90	8.22	8.17	7.26	5.99	7.11	7.34	8.02	8.23	7.19	7.84	4.88	6.02	6.36	5.00	4.56	6.47	6.45	6.95	0.03	0.5
Na2O	3.86	3.90	3.92	4.00	3.86	3.93	3.66	3.82	3.60	3.59	3.82	3.80	4.38	4.01	4	4.43	4.66	4.14	4.17	3.86	0.02	0.6
K2O	1.43	1.46	1.2	1.24	1.35	1.43	1.27	0.98	0.92	0.92	1.34	1.11	1.91	1.32	1.48	1.71	1.93	1.29	1.40	1.43	0.01	0.8
P2O5	0.97	0.98	0.43	0.47	0.59	0.22	0.20	0.25	0.19	0.19	0.30	0.41	0.19	0.17	0.18	0.17	0.17	0.23	0.20	0.98	0.01	1.1
Total	99.4	99.9	100.6	100.4	99.5	99.5	99.2	100.0	99.7	100.2	99.1	99.4	99.9	99.0	100.1	100.6	100.4	101.1	100.2	99.4	0.82	0.8
Mg #	59.8	59.2	65.2	64.7	66.9	67.6	70.7	67.0	70.4	70.8	69.4	66.3	60.7	70.0	73.9	65.2	58.1	71.4	68.4			
Trace element, ppm																						
Be	2.6	2.5	1.8	2.1	2.4	1.4	1.3	1.4	1.0	1.0	1.6	1.6	1.8	1.4	1.4	1.8	2.0	1.7	1.4	2.5	0.1	4.3
Li	16.4	16.0	10.3	10.6	11.2	16.1	16.1	12.3	11.0	10.5	12.8	11.5	22.6	4.8	18.7	24.7	29.3	18.5	19.4	15.8	0.3	2.0
B	13.3	13.4	2.6	2.6	7.2	10.7	8.2	8.1	5.3	4.9	11.4	5.1	26.5	9.2	8.2	19.2	20.8	10.3	11.1	14.1	1.0	6.9
Sc	21.9	22.0	23.0	23.5	20.6	18.4	22.1	21.9	24.8	24.6	20.2	23.5	12.4	15.1	17.2	13.2	12.1	17.9	17.5	21.9	0.3	1.4
V	149	150	157	157	148	129	151	145	173	172	153	168	106	113	115	88	79	126	129	151	2	1.2
Cr	199	185	228	213	288	230	361	259	401	409	250	255	109	226	284	135	56	275	178	200	3	1.7
Co	27.7	27.1	34.7	34.0	33.3	22.1	29.3	35.0	34.8	34.3	29.9	35.2	16.3	22.1	24.7	16.8	12.5	26.2	23.1	27.7	0.3	0.9
Ni	100	95	106	97	157	109	140	139	142	142	115	114	52	110	160	91	32	144	71	100	1	0.6
Rb	30.0	30.4	13.7	17.9	23.4	36.9	25.9	18.4	18.4	18.2	29.1	16.6	58.3	34.8	30.9	45.2	50.9	29.79	32.2	30.0	0.5	1.7
Sr	525	522	557	553	533	434	420	444	368	364	547	483	445	442	586	462	473	496	499	525	9	1.7
Y	44.3	44.2	28.7	29.4	34.4	20.5	21.2	26.0	20.5	20.4	22.4	28.2	20.7	15.6	17.2	17.5	17.5	19.8	19.5	44.3	0.5	1.2
Zr	428	433	222	228	301	166	151	168	135	134	166	207	175	142	146	134	151	152	155	428	5	1.1
Nb	34.5	34.4	24.4	24.9	26.0	6.4	7.7	12.6	4.9	4.8	9.5	19.0	6.2	4.8	4.0	4.4	4.6	6.2	5.4	34.5	0.4	1.3
Cs	1.06	1.07	0.23	0.17	0.73	1.58	1.07	0.68	0.67	0.68	1.30	0.23	3.32	0.81	1.47	2.66	3.13	1.62	1.72	1.06	0.01	1.0
Ba	490	483	267	274	373	383	311	225	222	221	350	274	445	344	402	373	396	311	331	490	7	1.3
La	42.0	41.7	20.7	21.4	27.7	15.6	13.7	13.5	10.7	10.6	17.6	18.7	16.4	13.1	17.0	13.2	13.7	14.0	14.2	42.0	0.5	1.1
Ce	94.7	95.7	45.5	46.6	61.3	34.1	30.3	31.0	24.8	24.5	39.1	40.6	35.1	28.5	37.8	28.7	29.2	31.5	32.1	94.7	1.4	1.5
Pr	11.7	11.7	5.8	5.9	7.8	4.5	4.0	4.1	3.4	3.4	5.1	5.3	4.6	3.7	5.0	3.8	3.8	4.3	4.3	11.7	0.2	1.6
Nd	48.6	48.5	24.3	25.1	32.8	18.5	17.1	17.8	15.2	15.1	21.8	22.8	19.0	15.7	21.4	15.8	15.7	18.3	18.5	48.6	0.7	1.4
Sm	9.87	9.75	5.50	5.66	6.91	4.09	4.01	4.41	3.76	3.72	4.79	5.24	4.19	3.45	4.52	3.56	3.52	4.18	4.20	9.87	0.14	1.5
Eu	2.84	2.85	1.80	1.82	2.13	1.26	1.26	1.48	1.20	1.19	1.47	1.67	1.18	1.06	1.34	1.09	1.05	1.27	1.28	2.84	0.04	1.5
Gd	9.21	9.20	5.49	5.67	6.57	3.96	3.95	4.73	3.78	3.78	4.38	5.30	3.81	3.09	3.86	3.41	3.34	3.96	3.91	9.21	0.11	1.2
Tb	1.39	1.39	0.86	0.89	1.02	0.61	0.62	0.76	0.60	0.59	0.67	0.84	0.60	0.47	0.57	0.52	0.52	0.61	0.60	1.39	0.02	1.4
Dy	7.74	7.77	5.03	5.16	5.85	3.55	3.67	4.52	3.52	3.47	3.84	4.90	3.41	2.65	3.06	2.97	2.96	3.46	3.38	7.74	0.10	1.3
Ho	1.54	1.52	1.00	1.03	1.17	0.72	0.75	0.91	0.72	0.72	0.77	1.00	0.68	0.52	0.60	0.60	0.60	0.69	0.68	1.54	0.02	1.0
Er	4.22	4.22	2.77	2.86	3.21	2.00	2.09	2.52	2.02	2.02	2.12	2.76	1.88	1.42	1.67	1.69	1.68	1.91	1.86	4.22	0.04	1.0
Yb	3.88	3.90	2.55	2.61	3.03	1.92	2.00	2.34	1.90	1.88	2.00	2.52	1.82	1.38	1.57	1.62	1.62	1.80	1.79	3.88	0.06	1.4

Table 1. (continued)

	Alkaline Group						Transitional Group							Calc-alkaline Group										
	V Chichinautzin		V Suchiooc		V Xitle	V Cuatepel		Vs La Cima	Las Tetillas		C Tecajete	V Cajete	Popocatepetl Proper			Popocatepetl's Recent Eruptions Series (Since 1994)				Repeat Analyses of Samples ASC1_S[c]		
	ASC1_S	ASC1_A	ASC44	ASC44B	SX25	SPO60	SPO56	LaCima3	LT4	LT3	SPO58B	SCEN22	TP6	SPO38	TP10C	30 April 1996	30 December 1996	30 June 1997	22 January 2001		SD	RSD, %
Lu	0.59	0.59	0.39	0.40	0.45	0.29	0.31	0.36	0.29	0.29	0.30	0.39	0.27	0.21	0.24	0.25	0.25	0.27	0.27	0.59	0.01	1.3
Hf	8.1	8.1	4.7	4.8	5.9	4.0	3.7	3.9	3.4	3.3	3.9	4.4	4.5	3.6	3.5	3.5	3.9	3.71	3.7	8.1	0.1	1.4
Ta	1.79	1.83	1.42	1.46	1.45	0.42	0.46	0.75	0.30	0.30	0.58	1.11	0.47	0.35	0.26	0.34	0.36	0.40	0.34	1.79	0.02	1.2
Tl	0.17	0.17	0.06	0.06	0.07	0.18	0.18	0.11	0.10	0.10	0.21	0.09	0.48	0.26	0.23	0.46	0.33	0.25	0.28	0.17	0.00	2.5
Pb	7.7	7.9	3.5	3.5	5.1	6.4	5.4	3.8	4.0	3.9	5.4	3.7	9.1	6.0	6.9	8.1	8.7	5.9	6.6	7.6	0.2	2.4
Th	3.59	3.61	2.34	2.41	2.77	3.19	2.59	1.95	1.68	1.66	3.00	2.37	5.17	3.18	3.44	3.96	4.41	2.89	3.08	3.59	0.05	1.3
U	1.08	1.09	0.56	0.57	0.86	1.00	0.80	0.62	0.54	0.54	0.93	0.72	1.87	1.25	1.11	1.47	1.72	1.03	1.10	1.08	0.01	1.2

[a] Abbreviations are V, volcano; Vs, volcanoes; C, Cerro; SD, standard deviation; and RSD, relative standard deviation.
[b] Analysts are SMS, S. M. Straub; AL, A. LaGatta.
[c] Repeat analyses during period of measurements are n = 5 repeats for major elements, and n = 8 repeats for trace elements.

$Yb)_n$ ratios are indistinguishable in all three groups, and slightly lower than those of Basin and Range basalts (calc-alkaline: 1.52 ± 0.06, n = 27; alkaline: 1.57 ± 0.04, n = 22; transitional: 1.53 ± 0.09; n = 36; Basin and Range basalts: 2.00 ± 0.38, n = 75; Tb/Yb is normalized to C1 chondrite [*Sun and McDonough*, 1989]). Rather, the conformity in MREE/HREE ratios suggests a common mantle origin for the central MVB series. However, isotopic systematics do not provide unambiguous source constraints, as exemplified in the Sr-Nd isotope space (Figure 4). In this diagram, the central MVB series substantially overlaps with the field of mantle xenoliths found behind the volcanic front [*Heinrich and Besch*, 1992; *Luhr and Gomez-Aranda*, 1997; *Nimz et al.*, 1993, 1995], but are also bracketed by slab and crustal compositions. Thus material from all of these sources can be involved, and quantifying that involvement is dependent on fully knowing the isotopic variability of the crustal basement and subarc mantle beneath the central MVB – a difficult condition. Similar ambiguities are evident in the Pb and Hf isotope spaces [*Cai et al.*, 2007; *LaGatta*, 2003]. On the other hand, the unusually Ni-rich olivines common in these central MVB series melts may provide a powerful tracer that helps unravel their origin and formation.

3. Olivine in Central MVB Andesites

[6] Olivine is a common phenocryst in central MVB volcanic rocks [e.g., *Schaaf et al.*, 2005; *Siebe et al.*, 2004a; *Straub and Martin-Del Pozzo*, 2001; *Wallace and Carmichael*, 1999]. It is the single phenocryst in the sparsely phyric basalts and basaltic andesites from the monogenetic volcanoes, and commonly present next to minor amounts of plagioclase and pyroxenes in the more evolved compositions [*Schaaf et al.*, 2005; *Siebe et al.*, 2004a]. Olivine is also the dominant phenocryst in the basaltic andesites and mafic andesites from the stratovolcanoes, and it is often present in trace amounts in their more siliceous compositions as residual component of in-mixed, mafic melts [e.g., *Nixon*, 1988a; *Schaaf et al.*, 2005; *Straub and Martin-Del Pozzo*, 2001].

[7] The selected sample suite is representative of the central MVB series (Figure 2 and Table 1). Bulk rock ranges from 51 to 65 wt % SiO_2 at MgO abundances of 8.1 to 2.0 wt %, and Mg # of 53 to 72. Samples were selected for the presence of olivine that is always the dominant, and in most cases, only phenocryst. Only in the most siliceous

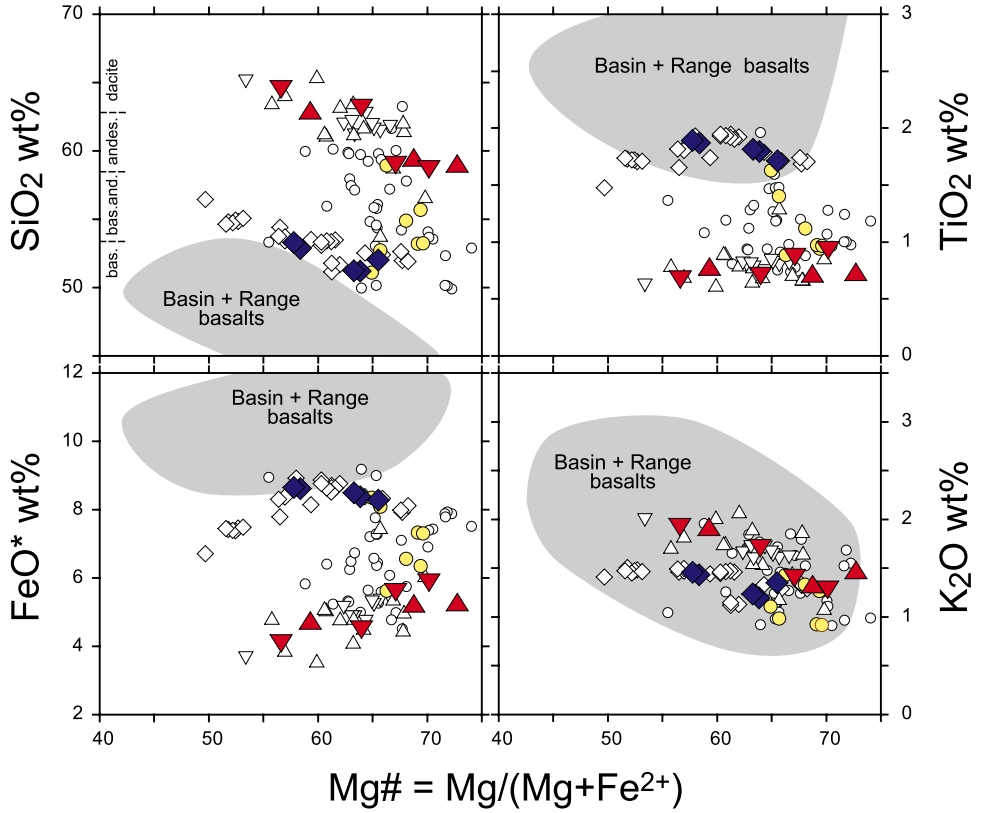

Figure 2. Selected major elements data of central MVB melts. Colored symbols are samples studied (Table 1); open symbols are data from *LaGatta* [2003] and from S. M. Straub et al. (Constraints on subarc mantle processes from clustered monogenetic cinder cones in the central Sierra Chichinauztin, Mexico, manuscript in preparation, 2008). Data range covered by open symbols coincides with data previously published from this area by *Siebe et al.* [2004a] and *Schaaf et al.* [2005]. Data for Mexican Basin and Range basalts (behind-the-front region of Mexican Volcanic Belt) are after *Luhr et al.* [1989, 1995a, 1995b] and *Gomez-Tuena et al.* [2003].

andesite samples of Popo, olivine phenocrysts are subordinate (sample TP6, and tephra from recent eruptions). Olivine phenocrysts range between 0.25 to 1.0 mm in size. Larger grains (0.5–1.0 mm fraction) are typically normally zoned with a broader homogenous core and a narrow, fosteritic rim lower by a few mole % (Tables 2 and 3). No inverse zoning has yet been reported [*Schaaf et al.*, 2005; *Siebe et al.*, 2004a; *Straub and Martin-Del Pozzo*, 2001], but in some dacitic samples from Popo, reaction rims of orthopyroxene have been observed. The ubiquitous inclusions of Cr-spinel and occasional sulfides emphasize the primitive character of the olivines [e.g., *Siebe et al.*, 2004a; *Straub and Martin-Del Pozzo*, 2001; *Straub et al.*, 2004].

3.1. Relationship Between Olivine and Bulk Rock

[8] Figure 5 shows that the Mg # of bulk rock correlates well with the Mg # values of melts in equilibrium with the olivine phenocrysts (=Mg $\#_{oliv}$). (Note that bulk rock Mg # are as measured, except for Popo's recent eruption series for which the most mafic tephra measured was used for the olivines from all four samples). The Mg $\#_{oliv}$ has been calculated from the average olivine core composition per sample using the experimentally established K_D^{Fe-Mg} [e.g., *Roeder and Emslie*, 1970]. Most of the samples plot within or close to equilibrium using the range of the experimentally determined K_D^{Fe-Mg} [*Falloon et al.*, 2007; *Putirka*, 2005; *Roeder and Emslie*, 1970]. The best correlation in Figure 5 is obtained for an exchange coefficient K_D^{Fe-Mg} of 0.32 (R^2 = 0.86, slope = 1.0). The strong correlation across the compositional spectrum of the central MVB melts suggests that the olivines investigated are in or close to equilibrium with bulk rock. The average Fo indeed reflects a key difference between alkaline and calk-alkaline end-member melts: Forsterite contents are systematically lower in the Fe-rich, low-Mg # alkaline melts than in the Fe-depleted high-Mg #

Table 2 (Representative Sample). Olivine Compositions [The full Table 2 is available in the HTML version of this article at http://www.g-cubed.org]

Sample ID	Volcano[a]	EMPA[b]	Reheat[c]	Zone[d]	Olivine ID[e]	Grain[f]	SiO_2, wt %	MgO, wt %	FeO, wt %	NiO, wt %	Ni, ppm	Total	Fo
SPO58	C Tecajete	AMNH	no	rim	spo58_ol1	1	38.8	38.6	18.82	0.059	464	96.2	78.5
SPO58	C Tecajete	AMNH	no	rim	spo58_ol1	1	39.1	43.2	16.57	0.053	416	98.9	82.3
SPO58	C Tecajete	AMNH	no	rim	spo58_ol1	1	39.6	44.9	14.72	0.053	417	99.2	84.5
SPO58	C Tecajete	AMNH	no	core	spo58_ol1	1	39.4	45.6	14.17	0.083	652	99.3	85.2
SPO58	C Tecajete	AMNH	no	core	spo58_ol1	1	39.8	46.5	12.61	0.202	1588	99.1	86.8
SPO58	C Tecajete	AMNH	no	core	spo58_ol1	1	40.2	47.4	11.95	0.301	2366	99.8	87.6
SPO58	C Tecajete	AMNH	no	core	spo58_ol1	1	39.8	46.1	13.2	0.214	1682	99.3	86.2
SPO58	C Tecajete	AMNH	no	core	spo58_ol1	1	40	45.5	13.57	0.211	1658	99.3	85.7
SPO58	C Tecajete	AMNH	no	core	spo58_ol1	1	39.7	45.4	14.01	0.125	982	99.2	85.2
SPO58	C Tecajete	AMNH	no	core	spo58_ol1	1	39.9	45.5	13.77	0.185	1454	99.4	85.5
SPO58	C Tecajete	AMNH	no	core	spo58_ol1	1	39.9	46.7	12.67	0.214	1682	99.4	86.8
SPO58	C Tecajete	AMNH	no	core	spo58_ol1	1	40	46.7	12.72	0.182	1431	99.6	86.7
SPO58	C Tecajete	AMNH	no	core	spo58_ol1	1	39.7	46.3	13.44	0.111	872	99.5	86
SPO58	C Tecajete	AMNH	no	rim	spo58_ol1	1	39	43.8	15.93	0.062	487	98.8	83
SPO58	C Tecajete	AMNH	no	rim	spo58_ol2	2	40	45	14.34	0.056	440	99.4	84.8
SPO58	C Tecajete	AMNH	no	rim	spo58_ol2	2	40	45.8	13.64	0.115	904	99.5	85.7
SPO58	C Tecajete	AMNH	no	rim	spo58_ol2	2	39.4	44.4	15.46	0.091	715	99.4	83.7
SPO58	C Tecajete	AMNH	no	core	spo58_ol2	2	40.2	46.4	12.65	0.24	1886	99.4	86.7
SPO58	C Tecajete	AMNH	no	core	spo58_ol2	2	40.4	47.4	11.71	0.416	3270	99.9	87.8
SPO58	C Tecajete	AMNH	no	core	spo58_ol2	2	40	46.4	13.09	0.136	1069	99.6	86.3
SPO58	C Tecajete	AMNH	no	rim	spo58_ol2	2	39.9	45.4	13.76	0.124	975	99.2	85.5
SPO58	C Tecajete	AMNH	no	core	spo58_ol2	2	40.1	47.2	11.98	0.229	1800	99.6	87.5
SPO58	C Tecajete	AMNH	no	core	spo58_ol2	2	39.9	46.3	12.53	0.169	1328	98.8	86.8
SPO58	C Tecajete	AMNH	no	rim	spo58_ol2	2	39.5	46	13.8	0.106	833	99.4	85.6
SPO58	C Tecajete	AMNH	no	rim	spo58_ol2	2	38	45.2	14.93	0.076	597	98.1	84.4
SPO58	C Tecajete	AMNH	no	rim	spo58_ol3	3	39.1	42.7	16.76	0.064	503	98.5	81.9
SPO58	C Tecajete	AMNH	no	core	spo58_ol3	3	39.7	44.9	14.28	0.09	707	98.9	84.9
SPO58	C Tecajete	AMNH	no	core	spo58_ol3	3	39.7	44.8	14.47	0.072	566	99.1	84.7
SPO58	C Tecajete	AMNH	no	core	spo58_ol3	3	39.6	44.5	14.97	0.049	385	99.1	84.1
SPO58	C Tecajete	AMNH	no	core	spo58_ol3	3	39.7	44.8	15.14	0.068	534	99.6	84.1
SPO58	C Tecajete	AMNH	no	rim	spo58_ol3	3	39.8	44	15.08	0.078	613	98.9	83.9
SPO58	C Tecajete	AMNH	no	core	spo58_ol3	3	39.9	45.3	13.49	0.164	1289	98.9	85.7
SPO58	C Tecajete	AMNH	no	core	spo58_ol3	3	39.8	45.8	13.42	0.165	1297	99.2	85.9
SPO58	C Tecajete	AMNH	no	core	spo58_ol3	3	40.1	45.8	13.44	0.155	1218	99.5	85.9
SPO58	C Tecajete	AMNH	no	core	spo58_ol3	3	39.9	45.4	13.81	0.125	982	99.2	85.4
SPO58	C Tecajete	AMNH	no	core	spo58_ol3	3	39.8	45.9	13.37	0.166	1305	99.2	86
SPO58	C Tecajete	AMNH	no	core	spo58_ol3	3	39.7	45	14.3	0.06	472	99.1	84.9
SPO58	C Tecajete	AMNH	no	core	spo58_ol3	3	39.7	44.6	14.65	0.032	252	99	84.4
SPO58	C Tecajete	AMNH	no	core	spo58_ol3	3	39.5	45.2	14.57	0.046	362	99.4	84.7
SPO58	C Tecajete	AMNH	no	rim	spo58_ol3	3	39	42.2	17.81	0.085	668	99	80.8
SPO38	Popo	AMNH	no	core	spo38_ol1	4	40	44.6	14.73	0.309	2429	99.7	84.4
SPO38	Popo	AMNH	no	core	spo38_ol1	4	40	46.6	12.87	0.25	1965	99.7	86.6
SPO38	Popo	AMNH	no	core	spo38_ol1	4	39.7	45	14.49	0.183	1438	99.4	84.7
SPO38	Popo	AMNH	no	rim	spo38_ol1	4	39.3	43	16.81	0.191	1501	99.3	82
SPO38	Popo	AMNH	no	rim	spo38_ol1	4	39.4	43.4	16.78	0.194	1525	99.8	82.2
SPO38	Popo	AMNH	no	core	spo38_ol1	4	39.4	44.3	14.94	0.209	1643	98.8	84.1
SPO38	Popo	AMNH	no	rim	spo38_ol1	4	39.1	42.1	16.01	0.306	2405	97.5	82.4
SPO38	Popo	AMNH	no	rim	spo38_ol2	5	39.7	45.5	13.59	0.271	2130	99.1	85.7
SPO38	Popo	AMNH	no	core	spo38_ol2	5	40.3	47.4	11.45	0.34	2672	99.5	88.1
SPO38	Popo	AMNH	no	core	spo38_ol2	5	40.3	48.1	10.82	0.398	3128	99.7	88.8
SPO38	Popo	AMNH	no	core	spo38_ol2	5	39.8	48	10.45	0.376	2955	98.6	89.1
SPO38	Popo	AMNH	no	core	spo38_ol2	5	39.6	47.5	10.42	0.361	2837	97.9	89
SPO38	Popo	AMNH	no	core	spo38_ol2	5	40.1	48.2	10.95	0.342	2688	99.6	88.7
SPO38	Popo	AMNH	no	core	spo38_ol2	5	40.3	47.2	11.73	0.376	2955	99.6	87.8

[a] Sample and volcano as given in Table 1.
[b] Denotes EMPA lab: Geo, Geomar Research Center,Germany; AMNH, American Museum for Natural History, New York.
[c] Denotes whether olivine was reheated prior to analyses (see also description in section A1).
[d] Indicates zone analyzed in olivine. (Note that core analyses only are used in the discussion.)
[e] ID of individual olivine grain for a given bulk sample.
[f] Consecutive number of individual olivines analyzed.

Table 3. Repeatability and Accuracy of Electron Microprobe Analyses for Olivines[a]

	Olivine 174.1[b] (n = 80) (Geomar)			Olivine 174.1[b] (n = 88) (Lamont)		San Carlos Olivine[b] (n = 64) (Geomar)		
	Reference Value	This Study	s, %	This Study	s, %	Reference Value	This Study	s, %
SiO_2	40.5	40.8	0.7	40.2[c]	1	40.81	40.75	0.4
FeO*	9.35	9.36	0.9	9.98[c]	0.9	9.55	9.55	0.9
MgO	49.2	49.8	0.7	49.6	1.2	49.42	49.23	1
NiO	0.36–0.40[d]	0.39	2.5	0.37	5	0.37	0.38	4
Total	99.54	100.5				100.29	100.22	
Fo[e]	90.3	90.5	0.1	89.9[c]	0.2	90.2	90.2	0.3

[a] All oxides abundances are given in wt %. The number of repeat analyses performed (n) is indicated. Precision (s %) is reported as the percentage of one standard deviation of n repeat analyses.
[b] Olivine 174.1 is a natural olivine from a lherzolite nodule from Kamoolda stream, Kauai, Hawaii (donated by R. W. White, courtesy of Albert Leger). Reference values are recommended AMNH in-house values. Smithsonian standard USNM 111312/444 (San Carlos olivine) was used to monitor Ni precision and abundances at the GEOMAR.
[c] SiO_2 and FeO* data obtained at Lamont, and FeO* data obtained at the American Museum of Natural History in New York (AMNH), (and thus Fo) were corrected by multiplying SiO_2 with 1.0137, and FeO* with 0.9379. After correction, Fo values are comparable within the error (for more details see S. M. Straub et al., Evidence for melt mixing in young volcanic rocks of the Sierra Chichinautzin volcanic field, central Mexico, manuscript in preparation, 2008).
[d] Not homogenous for NiO – NiO reported either to be 0.40 wt % or 0.36 wt % by different analysts (A. Leger, personal communication, 1997).
[e] Fo is atomic ratio of $Mg/(Mg+Fe^{2+}) * 100$.

calc-alkaline melts. The only exception is calc-alkaline sample (TP6) that has low Mg $\#_{oliv}$ and low Mg #. This sample is somewhat atypical in that it is a Ni-poor siliceous andesite of the Popo summit cone (62.9 wt % SiO_2; Ni = 52 ppm), where olivines have reaction rims of orthopyroxene. Thus mineral-melt equilibrium in TP6 is likely controlled by processes other than those that govern the more primitive melts.

[9] The strong correlation of Fo (or Mg $\#_{oliv}$) versus Mg # of bulk rock is surprising since there are many factors that disturb this equilibrium, such as magma mixing, variable melt oxygen fugacities and meltwater content. The central MVB series are clearly influenced by magma mixing [e.g., *Schaaf et al.*, 2005; *Straub and Martin-Del Pozzo*, 2001; *Straub et al.*, 2004]. Melt mixing is apparent by the Fo of olivines cores from the alkaline basalts ASCI_S and ASCI_A investigated, for which a large number of olivine grains were analyzed. The Fo is bimodally distributed (Figure 6) whereby neither maximum, at ~79.5–80 mole % and ~83–84 mole %, respectively, is in equilibrium with the bulk rock. The overall average of all olivines, however, is close to equilibrium (Figure 5). These

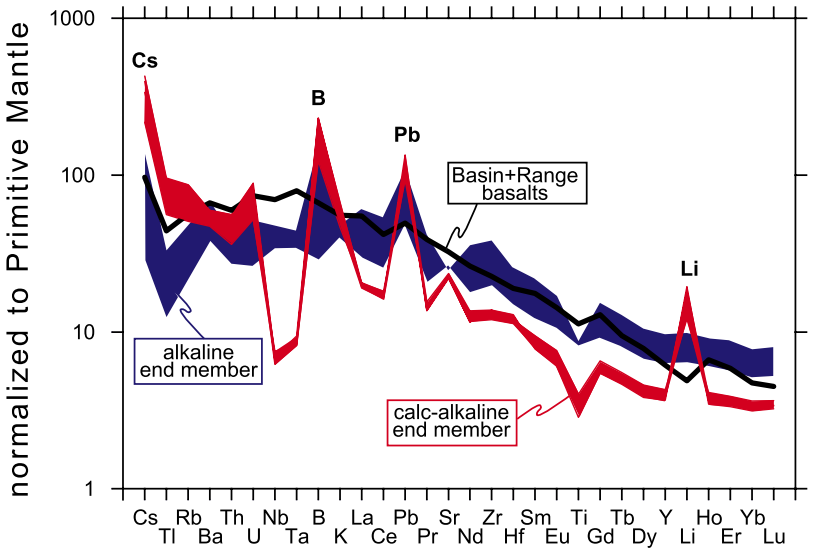

Figure 3. Incompatible trace element patterns of alkaline (blue) and calc-alkaline (red) end-member series compared to average (n ≤ 71 samples) of Mexican Basin and Range basalts (thick black line). Data sources are as given for Figure 2. For clarity, only calc-alkaline and alkaline end-members of the central MVB series are shown.

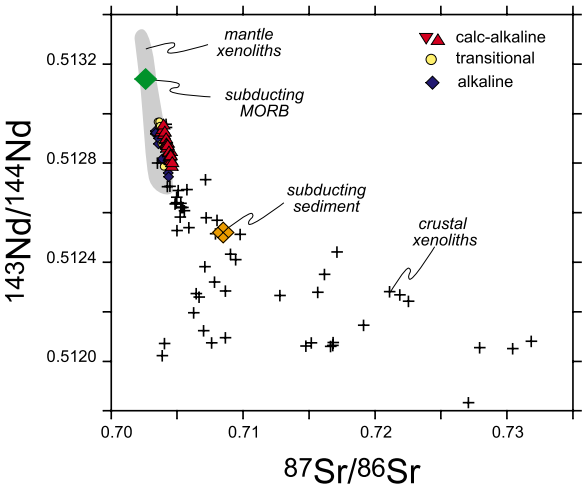

Figure 4. Sr versus Nd isotope ratios of central MVB series compared to slab, mantle, and crustal compositions. Unless denoted, sample symbols are as in Figure 1. Data sources for isotope data are as follows: central MVB series [*LaGatta*, 2003]; mantle xenoliths from the Mexican Basin and Range Province [*Heinrich and Besch*, 1992; *Luhr and Gomez-Aranda*, 1997; *Nimz et al.*, 1993, 1995]; and crustal xenoliths from within the MVB and adjacent basement outcrops [*Gómez-Tuena et al.*, 2003; *Lawlor et al.*, 1999; *Martinez-Serrano et al.*, 2004; *Roberts and Ruiz*, 1989; *Ruiz et al.*, 1988b, 1988a; *Schaaf et al.*, 1994].

samples are best interpreted as being hybrids of two component melts with slightly different Mg # (~54 versus 60) that mixed prior to eruption. Magma mixing is also evident in the Popo's recent eruption series [*Straub and Martin-Del Pozzo*, 2001]. In these melts, fosteritic olivines demonstrably represent a high-Mg # component melt that is balanced by a low-Mg # component melt preserved in the pyroxenes [*Straub and Martin-Del Pozzo*, 2001]. Mixing of component melts that are not fully represented by the olivines analyzed obviously contribute to deviations from ideal mineral equilibrium in Figure 5 (e.g., samples from Popo's eruption on 30 April and December of 1996). However, while magma mixing may cause deviation from equilibrium, it apparently has no potential to destroy the fundamental relationship between Fo and melt Mg # shown in Figure 5.

[10] The influence of variable oxygen fugacities and contents of meltwater appears similarly minor. Cr-spinels included in olivines from all three series indicate a melt $Fe^{3+}/\Sigma Fe = 0.18 \pm 0.04$, calculated after *Maurel and Maurel* [1982]. The oxygen fugacities of the magmas range between −0.5 and 1.5 relative to FMQ, based on the bulk rock compositions, the regression parameters of *Kilinc et al.* [1983] and temperatures of crystallization between ~1100° to 1200°C (calculated anhydrous after *Roeder and Emslie* [1970]). This range is very similar to *Wallace and Carmichael* [1999] based on the $Fe^{3+}/\Sigma Fe$ of whole rocks. The effect of f_{O2} is thus negligible, since a change in one log unit f_{O2} changes the K_D^{Fe-Mg} by only 0.02. The meltwater content varies widely in the central MVB (~1.3 to 5.6 wt % H_2O [*Atlas et al.*, 2006; *Cervantes and Wallace*, 2003a, 2003b]). However, there is no correlation apparent between meltwater and f_{O2}, nor is there evidence to date that the content of meltwater significantly changes the K_D^{Fe-Mg} [e.g., *Toplis*, 2005].

3.2. Ni Abundances in Olivine and Host Melts

[11] Figure 7 compares the Ni abundances of the central MVB olivines with olivines from mid-ocean ridge basalts (MORB), komatiites and volcanoes on thick lithosphere (>70 km) [*Sobolev et al.*, 2007]. The MVB olivines have a similar large range in Ni (0.03 to 0.53 wt %), but follow steeper and separate trends versus Fo. Their Ni maxima surpass the most Ni-rich olivines reported by *Sobolev et al.* [2005, 2007] at similar Fo (Fo_{83} to Fo_{90}). *Sobolev et al.* [2005] suggested that high-Ni olivines crystallize from mafic parental melts that are unusually rich in Ni (700–1000 ppm at 17–13.5 wt % MgO). However, the central MVB magmas do not require such high Ni abundances, given their low-MgO contents (~2–8 wt % MgO). At low MgO, the Kd_{Ni} is significantly higher than in melts with MgO >10 wt %, owing to the well-documented exponential increase of olivine Kd_{Ni} with decreasing MgO (Figure 8) [*Beattie et al.*, 1991; *Hart and Davis*, 1978; *Kinzler et al.*, 1990; *Leeman and Lindstrom*, 1978; *Leeman and Scheidegger*, 1977]. If Kd_{Ni} of olivines are as high as ~10–20, high-Ni olivines are in equilibrium with melt of only moderate Ni abundances (~75–240 ppm Ni, on average 150 ± 50 ppm Ni). These abundances compare fairly well with the measured Ni content of central MVB bulk rock (50–160 ppm Ni, average of 118 ± 28 ppm), as it can be expected if the olivines are nearly equilibrated with bulk rock.

[12] The Ni abundances in the melts are still sufficiently high to imply a mantle origin. Ni is strongly enriched in the mantle (~1800–2000 ppm in bulk mantle) but depleted in the continental and oceanic crust (~50–200 ppm; see also http://www.petdb.org [*Rudnick and Gao*, 2002]). Ni is not mobile in fluids, nor is mobilized in low-MgO,

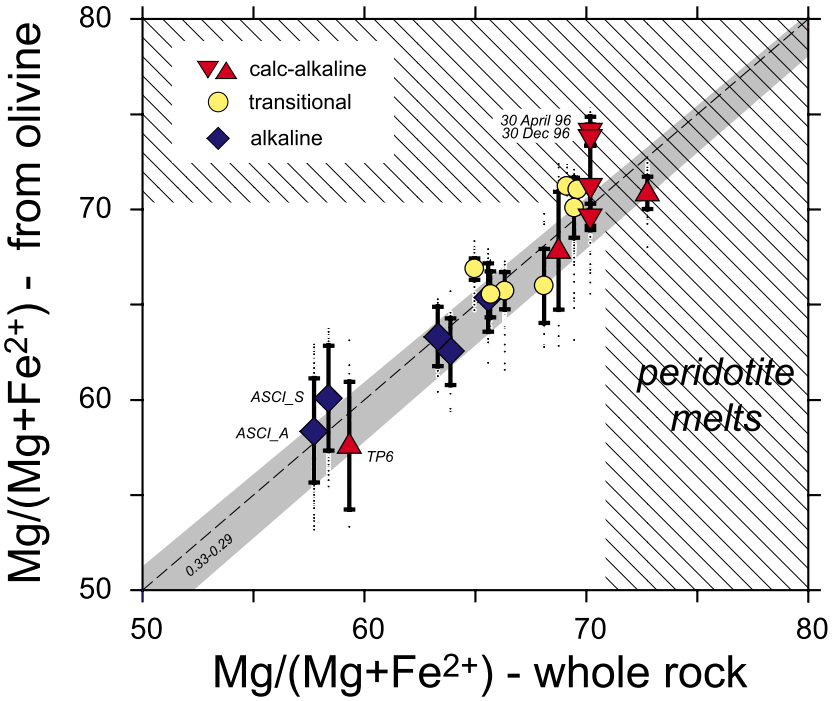

Figure 5. Mg # of bulk rock versus Mg $\#_{oliv}$ calculated from average of olivines per sample. The calculation uses an olivine $K_D^{Fe-Mgo} = 0.32$ and a ferric/ferrous ratio of 0.18 ± 0.04 based on included Cr-spinel [*Maurel and Maurel*, 1982]. Sample symbols are as in Figure 1. Grey band indicates acceptable range of olivine $K_D^{Fe-Mgo} = 0.29–0.33$ for anhydrous melts. Total error bars are 2 standard deviations of average Mg $\#_{oliv}$ per sample. Black dots are Mg $\#_{oliv}$ from individual olivine analyses (n = 2006). Dashed line is regression through all olivine analyses (y = 0.995 * x; $R^2 = 0.86$; forced through origin). Hatched field shows range of olivine in equilibrium with peridotite. Mg # of bulk rock are as measured except Popo's recent eruption samples for which the most mafic tephra bulk composition measured was used for all tephra samples. See text for discussion.

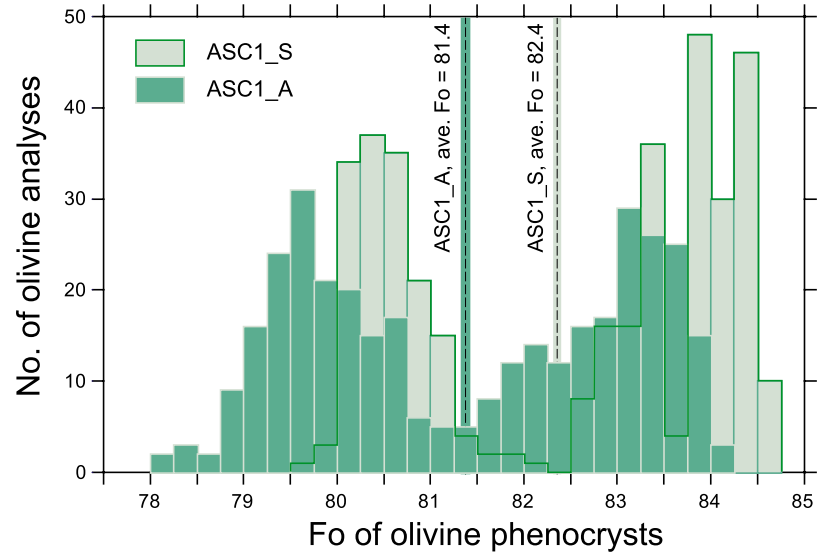

Figure 6. Histogram of olivines measured in two different alkaline basalts ASC1_A and ASC_S. The bimodal Fo distribution suggests that the bulk rocks were hybrids since the overall Fo average is close to equilibrium with bulk rock. The mingled component melts differ mostly in Mg # (~54 versus 60), while melt inclusions in high-Ni and low-Ni olivines are indistinguishable in K_2O (~1.6 wt %) and K_2O/TiO_2 ratios (~0.7) from each other and similar to bulk rock. Therefore, the component melts should be cogenetic [*Straub et al.*, 2004].

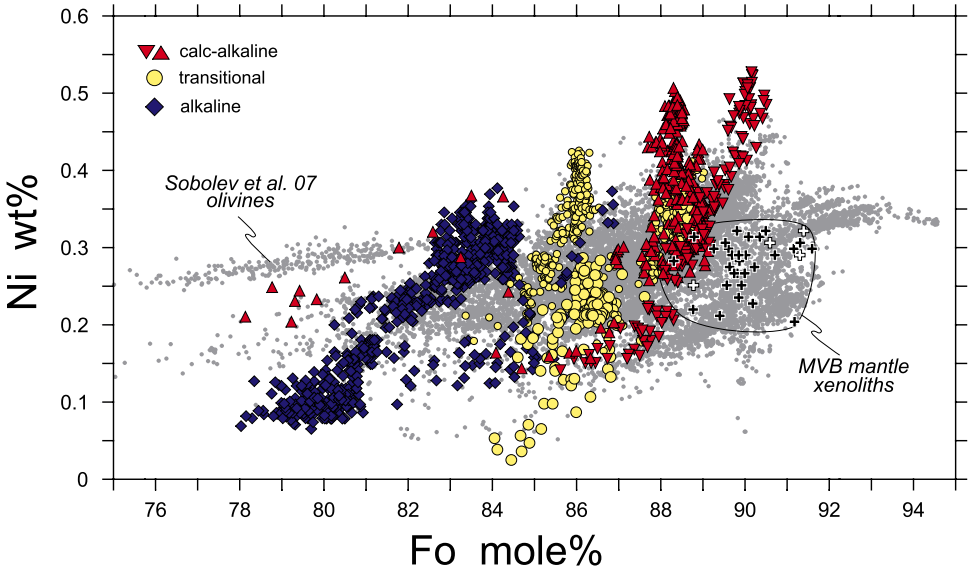

Figure 7. Ni versus Fo of central MVB olivines compared to olivines from mid-ocean ridge basalts (MORB) and komatiites and from volcanoes constructed on thick lithosphere (>70 km) after *Sobolev et al.* [2007]. (Olivine data from volcanoes on thin lithosphere add no more information and are omitted for clarity). Note that Ni in olivine is not given in NiO. Black crosses indicate olivine in mantle xenoliths from various locations from the Mexican Basin and Range Province [*Heinrich and Besch*, 1992; *Luhr and Gomez-Aranda*, 1997; *Nimz et al.*, 1993]. White crosses indicate olivine of mantle xenoliths at the volcanic front [*Blatter and Carmichael*, 1998a]. Other symbols are as in Figure 2.

siliceous partial melts. Slab or crustal partial melts have therefore low Ni (several 10 ppm at the most), because Ni is retained in residue, e.g., by pyroxene, a principal residual phase in slab and crust lithologies [*Beattie et al.*, 1991; *Ewart and Griffin*, 1994; *Seitz et al.*, 1999; *Villemant*, 1988; *Witt-Eickschen and O'Neill*, 2005]. In contrast, low-degree melts (1–2%) of fertile peridotite have a minimum of ~300–350 ppm melt Ni, that may double or triple as the extent of melting increases to 20–30%, or the source becomes more refractory by repetitive melting extraction (e.g., after up to 20–30% total melt extraction [*Langmuir et al.*, 1992]). Consequently, the subarc mantle is the most likely source of the primitive parental melts of all three compositional groups. Could the central MVB basaltic andesite and andesite be primary melts as suggested by *Blatter and Carmichael* [1998b, 2001]?

3.3. A Fundamental Problem

[13] This simple concept of a mantle origin, however, meets with a fundamental problem: partial melts from peridotite that crystallize olivine upon ascent cannot combine low-MgO abundance (~2–8 wt % MgO) at the given Ni abundances (~75–240 ppm). This is evident in the Ni versus Fo diagram (Figure 9) where melt evolution is strictly constrained with respect to MgO, FeO and Ni, because (1) the K_D^{Fe-Mg} is a constant [*Putirka*, 2005; *Roeder and Emslie*, 1970], and (2) the olivine $Kd_{Ni\text{-}oliv}$ is a well-defined function of the MgO content of the melt [*Beattie et al.*, 1991; *Hart*

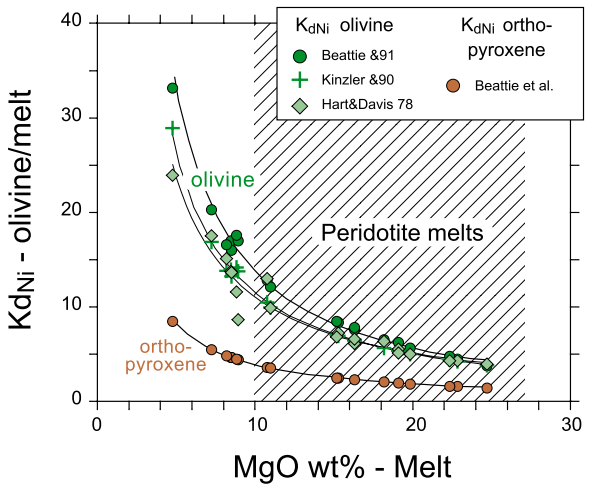

Figure 8. Dependence of Kd_{Ni} of olivine and orthopyroxene on melt compositions. Olivine Kd_{Ni} is after *Hart and Davis* [1978], *Beattie et al.* [1991], and *Kinzler et al.* [1990]. Orthopyroxene Kd_{Ni} is after *Beattie et al.* [1991]. Hatched field shows melt in equilibrium with peridotite that has at least 10 wt % MgO, which keeps Kd_{Ni} comparatively low.

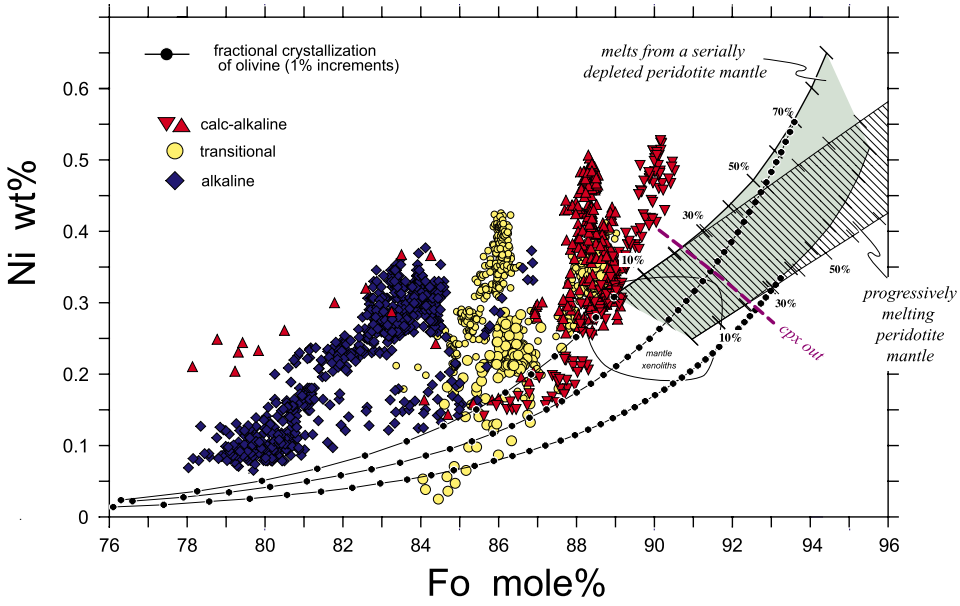

Figure 9. Ni versus Fo of central MVB olivines compared to range of partial melts from peridotite. A range of mantle compositions is assumed based on the xenolith data (see Appendix A for more modeling details). Green field shows range of melts is created from serially melting peridotite, assuming melt extraction in 2% step for a total extraction of up to 90% (approximates fractional melting). Hatched field indicates range of melts generated by variable extent of melting (0–70%) form a single source. Lilac line indicates approximate point of clinopyroxene consumption (after ~20–22% melt extraction) that should effectively terminate melting.

and Davis, 1978; *Kinzler et al.*, 1990]. In other words, the relative proportions of FeO, MgO and Ni in the melt (but not their abundances) are preserved by the Fo and Ni of olivine. The trends in Figure 9 constrain without doubt that partial melts from peridotite, even highly depleted peridotite, that crystallize olivine during ascent, cannot generate the host melts of the Ni-rich olivines. They may, however, produce melts that crystallize low-Ni olivines. For example: a peridotite mantle with olivines of Ni = 2800 ppm produces a partial melt of at least ~10 wt % MgO, but not more than ~280 ppm Ni, given an olivine Kd_{Ni} of ~10 (Figure 8). (Since >80% of Ni in peridotite is stored in olivine, olivine will control Ni abundance of melt; see appendix for more details). If olivine crystallizes first, this melt cannot crystallize olivine with more than 2800 ppm Ni. Since olivine crystallization depletes the melt rapidly in Ni and MgO, it is impossible to maintain high-Ni values in low-MgO melts.

4. Origin of Central MVB Magmas: Magma Mixing Versus Melt-Rock Reaction Processes

[14] How else can melts be generated which combine low-MgO contents with moderate Ni contents? The central MVB series are comparable to other arcs with respect to oxygen fugacities and crystallization temperatures, and no unusual conditions of melt formation are apparent. The relatively low oxygen fugacities are consistent with the widespread occurrence of sulfide inclusions in mafic phenocrysts [e.g., *Blatter and Carmichael*, 2001], and sulfides inclusion in olivine were observed in some of the alkaline basalts investigated. Their existence argues against selective Ni enrichment by a possible oxidative decay of coexisting, immiscible Fe-S-O component melts. In addition, sulfur-rich melts form Ni-S complexes, which lower the Ni available for sequestration in olivine [*Li et al.*, 2003]. These melts should crystallize even lower-Ni olivines than S-poor melts. Rather, the ubiquity of Ni-rich olivines in a broad range of alkaline and calc-alkaline series suggests a silicate melt control of the Ni enrichment. Two possibilities exist to generate melts with sufficient Ni at low MgO abundances: (1) melt mixing and (2) melt–rock reaction processes.

4.1. Melt-Mixing Models

[15] A simple way to create suitable host melts is by mixing of Ni- and Mg-rich, high-Mg # peridotite melts with Ni-, Mg- and Fe-poor melts that have low Mg # values. Hybrids of such melts have

Table 4. End-Member Composition for Model Shown in Figures 10a and 10b[a]

	Melt MgO, wt %	Melt FeO, wt %	Melt Mg #	Melt Ni, ppm	Fo in Olivine	Olivine Kd_{Ni}	Ni in Olivine, ppm
Mantle melt (22%)[a]	17.1	10.3	74.7	609	90.9	6.3	3859
Mantle melt (80%)[b]	20.4	7.7	82.5	1172	94.1	5	6076
Derivative melt (35%)[b]	4.7	9.1	47.9	11	75.7	26	273
Derivative melt (46%)[c]	3.4	6.4	49.1	6	76.6	35	203

[a] For modeling details, see Appendix A.
[b] Melt in equilibrium with peridotite mantle after total melt extraction of 22% or 80% by serial melting in 2% steps.
[c] Melt after 35% and 46% fractional loss of olivine from 22% and 80% mantle melts, respectively.

intermediate Ni, but a much higher Kd_{Ni} owing to the lower melt MgO, and hence may crystallize high-Ni olivine [e.g., *Straub et al.*, 2006; *Wang et al.*, 2006]. Suitable low-Mg # melts can be produced by (1) fractional crystallization of earlier ascending melt batches in the same volcano-magma system, or (2) by partial melting of slab and crust lithologies (Tables 4 and 5). Figures 10 and 11 illustrate that, by mixing partial melts of peridotite with low-MgO melts, hybrid melts with variable FeO/MgO ratios can be produced that are in equilibrium with high-Ni olivine. However, a more detailed examination of the data arrays reveals that, despite being mathematically possible, such melt-mixing models must be rejected because they cannot be reconciled with the related geochemical data.

[16] First, only few central MVB compositions plot along the primary mixing lines which exclude them from being direct mixing products (Figures 10 and 11). Rather, the MVB melts need to be derivative melts from fully hybridized, presumably crystal-free liquids prior to olivine precipitation. Second, most mixing models require a component melt from an extremely depleted mantle to maintain sufficient Ni in the hybrids. This extremely depleted mantle can only be created by repetitive melt extraction (Figure 9). The required total melt extraction of ~80% goes well beyond the exhaustion of clinopyroxene that should be lost from the source after ~20–22% melt extraction, and which would effectively terminate melting [e.g., *Langmuir et al.*, 1992; *Longhi*, 2002]. Furthermore, melts from an extremely depleted mantle are depleted in incompatible trace elements, and hence an unlikely mixing end-member for the enriched alkaline melts. *Leeman et al.* [2005] suggested that alkaline melts of the Cascades arc may be mixtures of a highly depleted, Ni-rich melt from depleted lithospheric mantle, and a larger proportion of low-Ni melts from a fertile asthenospheric mantle. However, this model can be ruled out for the central MVB, because melt inclusions in high-Ni and low-Ni olivines of the alkaline samples (marked in blue in Figure 10) have similar high-K_2O (~1.6 wt %) and low-K_2O/TiO_2 ratios (~0.7) as bulk rock [*Straub et al.*, 2004].

[17] Third, derivative melts are difficult to generate and remain unsatisfactory as mixing end-members. Melts from depleted mantle have high MgO and FeO abundances (e.g., a melt from a 20% depleted mantle has MgO = 17.1 wt % and FeO ~10.3 wt %; Tables 4 and 5). Such melts would need to crystallize and loose ~33–46% olivine in order to

Table 5. End-Member Compositions for Model Shown in Figures 11a and 11b[a]

	Melt MgO, wt %	Melt FeO, wt %	Melt Mg #	Melt Ni, ppm	Fo in Olivine	Olivine Kd_{Ni}	Ni in Olivine, ppm
Mantle melt 22%[b]	17.1	10.3	74.7	609	90.9	6.3	3859
Mantle melt 60%[b]	19.2	8.7	79.7	908	93.0	5.6	5040
Slab/crust melt[c]	0.5	2.0	30.8	10	60.2	247	2471
Slab crust melt[d]	5.0	15.0	37.3	100	66.8	24	2390

[a] For modeling details see Appendix A.
[b] Melt in equilibrium with peridotite mantle after total melt extraction of 22% or 80% by serial melting in 2% steps.
[c] Low-Fe, low-Mg partial melt from slab or crust with low Ni content.
[d] High-Fe, high-Mg partial melt from slab or crust with high Ni content, whereby range low degree of slab and crust melt is estimated based on experimental data by *Beard and Lofgren* [1991], *Johnson and Plank* [1999], *Kessel et al.* [2004], and *Rapp and Watson* [1995].

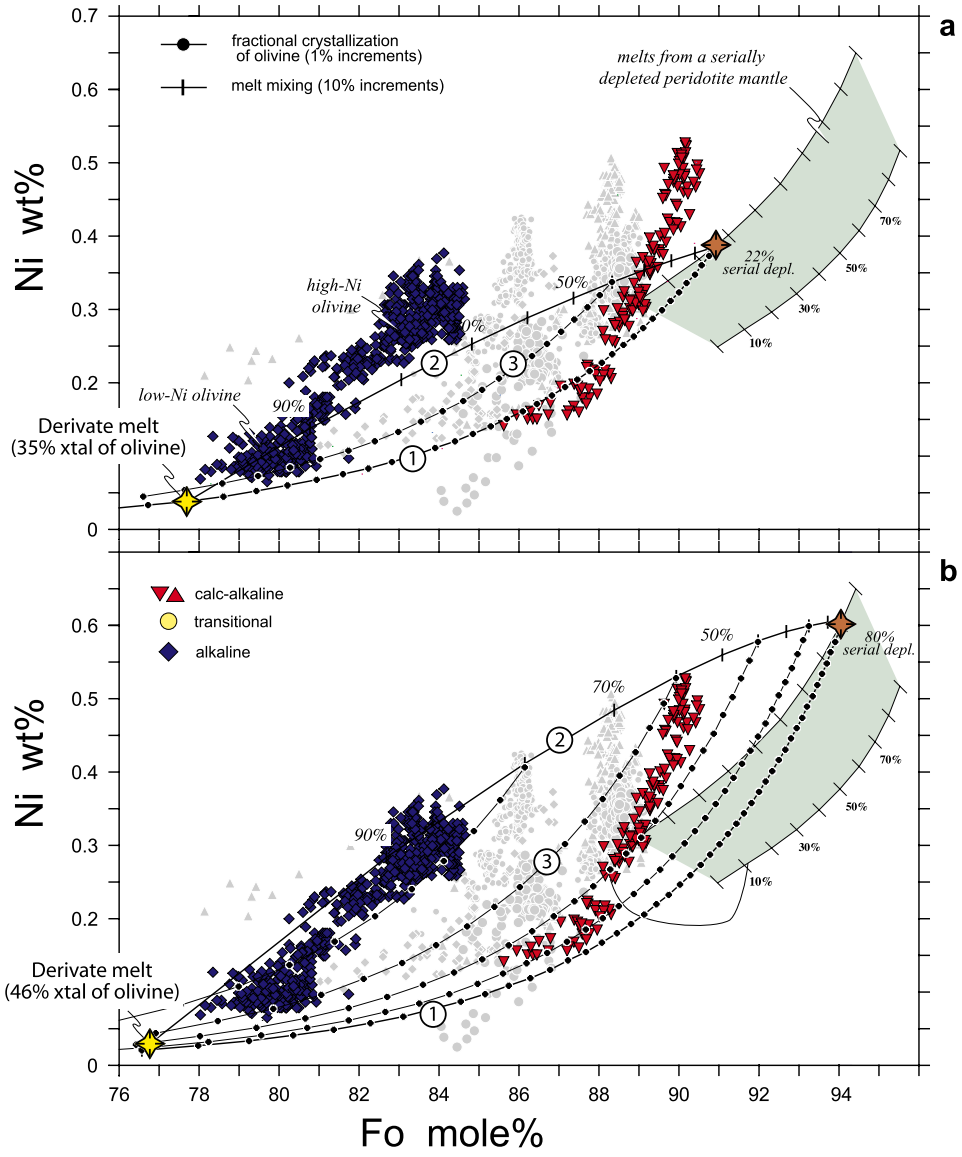

Figure 10. Ni versus Fo diagram illustrating mixing between partial melts from peridotite (orange stars) with derivative melts generated by olivine fractionation (yellow stars). For clarity, only end-members are highlighted in blue diamonds (alkaline) and inverted red triangles (calc-alkaline). The model assumes that first a derivative melt by fractional crystallization was created (line 1) that became mixed with later ascending melt in the magma plumbing systems (line 2). Mixing melt may fractionate olivine again (line 3). (a) Mafic end-member (orange star) 2% melt from a peridotite that has previously lost 10% melt by serial melt extraction mixes with derivative melt that has lost 35% olivine. (b) Mafic end-member (orange star) 2% melt from a peridotite that has previously lost 70% melt by serial melt extraction mixes with derivative melt that has lost 56% olivine. Table 4 lists examples of end-members and mixed melts. See text for discussion.

create a suitable end-member (Figure 10). Such a large loss, that would be even larger if pyroxene and plagioclase coprecipitated, is unsubstantiated. Low-degree partial melts from slab or crust lithologies do not provide acceptable end-members either. Because of the low FeO and MgO of these melts (a few wt % of MgO and FeO [*Beard and Lofgren*, 1991; *Johnson and Plank*, 1999; *Kessel et al.*, 2004; *Rapp and Watson*, 1995; *Yaxley and Green*, 1998]), a large proportion of several tens percent would be required (see mixing lines in Figure 11). Such mixing proportions are not supported by the Sr-Nd-Pb isotope signature of the MVB andesites (Figure 4) [*LaGatta*, 2003]. Partial slab and crust melts are also highly fractionated [e.g., *Kessel et al.*, 2004; *Rudnick and Gao*, 2002],

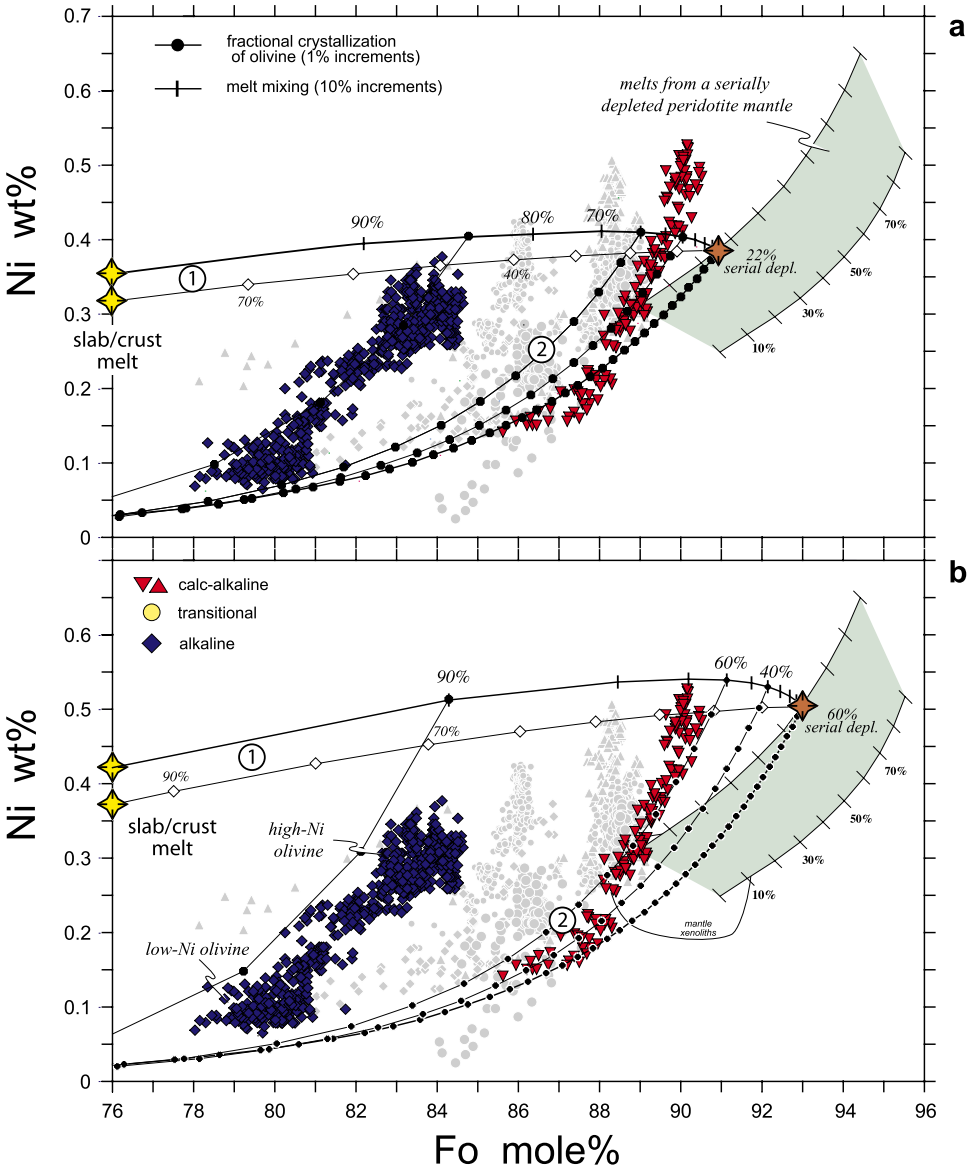

Figure 11. Ni versus Fo diagram illustrating mixing between partial melts from peridotite (orange stars) with low-degree melts from crust and slab lithologies (yellow stars). Two different compositions for slab/crust melts are considered based on experimental data [*Beard and Lofgren*, 1991; *Johnson and Plank*, 1999; *Kessel et al.*, 2004; *Rapp and Watson*, 1995]: (1) a low-Fe, low-Mg slab/crust melt with low Ni = 10 ppm (mixing line with solid diamonds) and (2) a high-Fe, high-Mg slab/crust melt with higher Ni = 100 ppm (mixing line with open diamonds). The model assumes that the slab/crust mixes first with the mantle melt (line 1) before producing derivative melts by fractional crystallization of olivine (line 2). Two different end members of mantle melts are exemplified: (a) Melt from mantle that has previously lost 22% melt by serial melting and (b) melt from mantle that has previously lost 60% by serial melting. Only a melt from such an extremely depleted mantle (unrealistically high) would have sufficient Ni to account for the most Ni-rich magmas of the central MVB. Table 4 lists examples of end-members and mixed melts. See text for discussion.

and cannot not create the comparatively flat patterns of the alkaline melts (Figure 3). Note that the alkaline end-member would require an even higher percentage of slab or crust melt (~70–90%) than the calc-alkaline end-member (50–60%), an unreasonable condition. In summary, melt-mixing models have serious problems. They may provide partial answers, but fail to provide a comprehensive, internally consistent model that accounts for the entire chemical spectrum observed.

4.2. Melt-Rock Reaction Processes

[18] When melts or fluids percolate through host rocks with which they are not equilibrated, chemical and mineralogical changes result (''melt-rock reaction''). The subducting slab readily produces hydrous siliceous fluids or melts (termed ''critical fluids'' by *Kessel et al.* [2004], and referred to as ''slab component'' hereinafter), that infiltrate the peridotite subarc mantle. Hence melt-rock reaction processes play a key role in many models of andesite petrogenesis [e.g., *Gómez-Tuena et al.*, 2007; *Kelemen et al.*, 2004; *Kelemen et al.*, 1998; *Liu et al.*, 2005; *Rapp et al.*, 1999; *Tatsumi*, 2001]. In essence, these models propose that the typical enrichment/depletion pattern of arc magmas (''arc signature'') is a blend of refractory elements assimilated from the mantle (e.g., Ni, Mg) and mobile elements added from the slab (e.g., Si, fluid mobile LILE, H_2O). The slab component mainly consists of H_2O (~56–83 wt %) and SiO_2 (12–31 wt %), in addition to significant amounts of Al_2O_3 (1.5–4.2 wt %), Na_2O (1–2.8 wt %) and fluid mobile LILE [e.g., *Kessel et al.*, 2004]. It reacts with peridotite and transforms mantle olivine to orthopyroxene (''reaction orthopyroxene''): $SiO_2 + (Fe, Mg)_2SiO_4 = (Mg, Fe)_2Si_2O_6$. This reaction has been well documented in experiments [e.g., *Hirschmann et al.*, 2006; *Sobolev et al.*, 2006; *Yaxley and Green*, 1998] and also in studies of mantle rocks [e.g., *Ertan and Leeman*, 1996; *Liu et al.*, 2005; *Porrera et al.*, 2006]. Formation of ''reaction orthopyroxene'' occurs in narrow (centimeter to decimeter scale?) reaction zones along the pathways of the percolating fluids that may be sharply bounded toward the unmodified mantle peridotite [e.g., *Liu et al.*, 2005; *Porrera et al.*, 2006]. If olivine is destroyed, a new pyroxenite lithology forms that is composed of newly formed orthopyroxene (''reaction orthopyroxene'') in addition to the original mantle orthopyroxenes and clinopyroxenes. Assuming a fertile peridotite with phase proportions of Oliv:Opx:Cpx:Grt of 55:19:23:2.2, orthopyroxene would then dominate the new lithology (~77 vol %, 2/3 of which are ''reaction orthopyroxene'') with lesser clinopyroxene (~23 vol %).

[19] Pyroxenites have lower solidi and higher melt productivity relative to peridotite at a given pressure [*Hirschmann and Stolper*, 1996]. Therefore they melt preferentially, and contribute disproportionately to the erupted melt volumes [*Hirschmann and Stolper*, 1996; *Sobolev et al.*, 2005]. A very important aspect is that pyroxenites may produce a range of low-MgO, siliceous andesitic melts (e.g., MgO ~2–10 wt % and SiO2 ~50–60 wt % [*Kogiso et al.*, 2004]), because olivine does not control SiO_2, MgO, FeO and Ni anymore. These melts should be enriched in Ni because the bulk partition coefficient D_{Ni} for pyroxenite is lower than that of peridotite [*Sobolev et al.*, 2005]. Such melts can also have high-Mg # values, dependent on the Mg # value of the protolith.

[20] The Mg # and Ni of partial melts from pyroxenite can be calculated (Figure 12, see Appendix A for modeling details). The calculation starts with the assumption that any amount of slab-derived FeO, MgO or Ni is insignificant compared to mantle abundances. This assumption is based on (1) experimental studies [e.g., *Johnson and Plank*, 1999; *Kessel et al.*, 2004] that show that neither MgO or FeO are mobilized at temperatures below 1000°C and (2) the inference that slab surface temperature are not above 800°C below central Mexico [*Manea et al.*, 2004]. From this it follows that ''reaction orthopyroxene'' must inherit the Mg # and Ni from the olivine. Consequently, the Mg # of the bulk pyroxenite is identical to that of the peridotite transformed. The Ni in pyroxenite, however, is lower because it is diluted by the added SiO_2 (~14–20% dilution, see appendix for details). In the pyroxenite, orthopyroxene has taken over the role as the main host of MgO, FeO and Ni. Therefore orthopyroxene will now control SiO_2, MgO, FeO, Mg # and Ni in partial melts. Partial melts from pyroxenite may have lower MgO and FeO and higher SiO_2 abundances [*Kogiso et al.*,

Figure 12. Genetic model illustrated in Ni_{oliv} versus Fo diagram. Symbols are as in Figure 1. Green field indicates peridotite mantle source that has lost up to ~20% melt by serial melting in 2% steps. Dashed lines indicate range beyond the exhaustion of clinopyroxene from source. Ochre field indicates pyroxenite mantle source that formed by melt-rock reaction processes from the peridotite mantle outlined by the green field. The pyroxenite lithology is assumed to produce melts with MgO ~4 to 10 wt %. (a) Olivines according to their major compositional groups. (b) Olivines distinguished from individual hand specimens. Samples TP6 (Popo summit cone) and alkaline basalts (ASC1_A and ASCI_S) plot outside the range covered by peridotite and pyroxenite melts and were likely formed by magma mixing. Since the nearly straight magma mixing lines require the MgO and FeO abundances of the mixing end-members to differ by only a few weight percent, magma mixing likely involves derivates of similar parental melt in the plumbing system (see text for discussion).

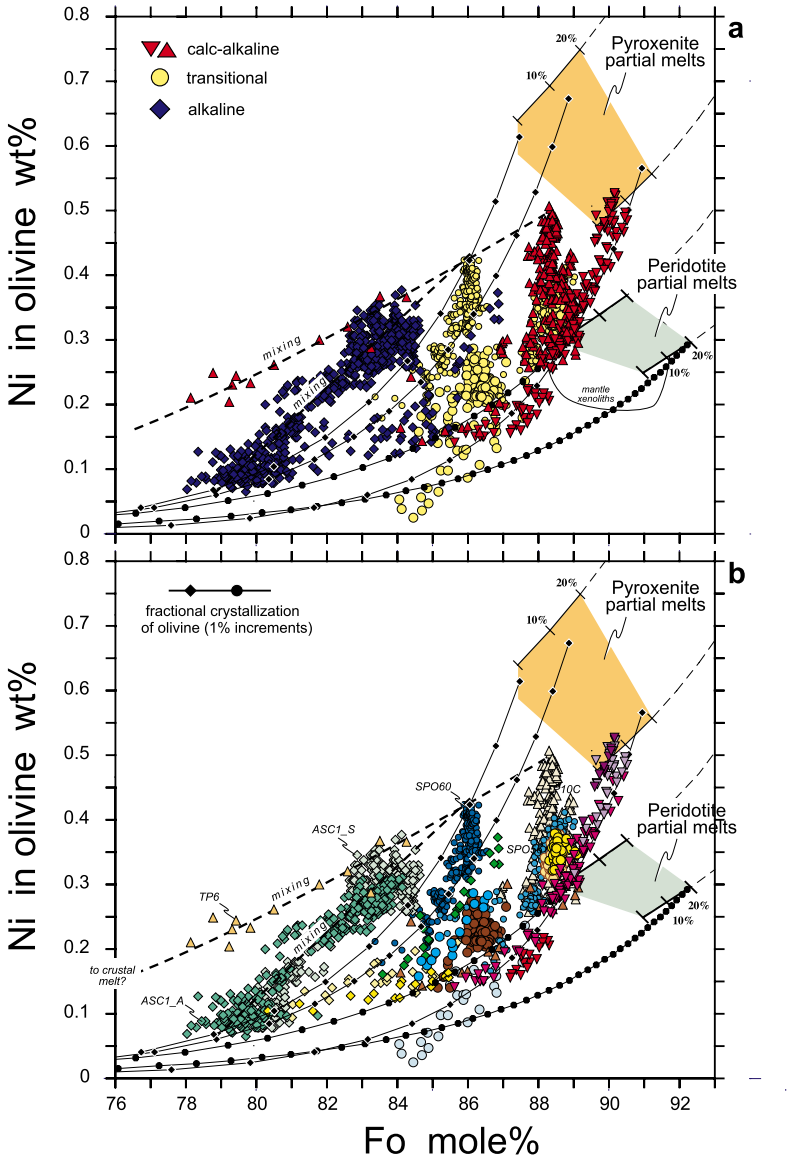

Alkaline

V. Chichinautzin
- ASC1_A
- ASC1_S

V. Suchiooc
- ASC44A
- ASC44B

V. Xitle
- SX25

Transitional

V. Tecajete
- SPO58

Vs. La Cima
- La Cima

V. Las Tetillas
- LT3
- LT4

V. Cuatepel
- SPO60
- SPO56

V. El Cajete
- SCEN22

Popocatepetl (calc-alkaline)

Popocatepetl proper
- TP6
- TP10C
- SPO38

Recent eruptions: 1996-2001
- 30 April 1996
- 30 Dec 1996
- 30 June 1997
- 22 Jan 2001

Figure 12

Table 6. Range of Melt Compositions Produced by Partial Melting of Peridotite and Pyroxenite Lithologies[a]

	Melt MgO, wt%	Melt FeO, wt %	Melt Mg #	Melt Ni, ppm	Fo in Olivine	Kd_{Ni} Olivine	Ni in Olivine, ppm
Peridotite[b]	~10–18	~7–10.6	~70–79	~176–526	89–92.7	~4–10	~2500–3780
Pyroxenite[c]	~4–10	~5.6–8.6	~67–76	~140–540	87.5–91.5	~12–37	~5000–7200

[a] See Appendix A for modeling details.
[b] Peridotite source is assumed to have lost up to 22% total melt by serial melting in 2% steps.
[c] Pyroxenite source is assumed to have formed from same peridotite depleted by melting.

2004], but given the fairly similar exchange coefficient for olivine (K_D^{Fe-Mg} ~0.295) and orthopyroxene (K_D^{Fe-Mg} ~0.255), only slightly lower Mg # values than melts of the peridotite that has been transformed. In addition, the pyroxenite melts will also be enriched in Ni (~140–540 ppm) because the Kd_{Ni} (~4–10) is ~3 times lower relative to olivine Kd_{Ni} (Figure 8). At a low primary melt MgO ~4–10 wt %, the Kd_{Ni} is sufficiently high to crystallize the fosteritic, high-Ni olivine typical of the central MVB series.

[21] Table 6 summarizes the range of primary melts produced from peridotite and pyroxenite lithologies. The modeling results are shown in Figure 12, with individual samples being highlighted in Figure 12b. Most of the olivines fall within the range of melt produced by olivine fractionation from either peridotite or pyroxenite primary melts. Primary pyroxenite melts need only loose a few percent of olivine, which suggests that the most Ni-rich olivines crystallize from near-primary melts. However, three samples cannot be related to primitive melts by only fractional crystallization. Two samples, the alkaline basalts ASC1_A and ASC1_S (green diamonds in Figure 12b), show strong evidence for mixing of cogenetic component melts (Figure 6). The third sample is a siliceous andesite (TP6) from Popo summit, which displays petrographic evidence of disequilibrium (reaction rims of orthopyroxene on olivines). If the samples are indeed hybrids, the MgO and FeO contents of the mixing end-members can differ only by a few wt %, because the mixing lines are nearly straight in the Ni versus Fo space (Figure 12b). This suggests mixing of different, possibly cogenetic magma batches, in the plumbing system that have lost variable amounts of olivine. For the alkaline basalts (ASC1_A and ASC1_S), a suitable low-Mg # end-member melt can be produced by as little as ~10% fractional crystallization of olivine from a primary parental melt. If this fractionated magma was still in the magma plumbing system, it could have mixed with later ascending, less fractionated melt batches prior to eruption. A larger amount of fractional crystallization is required for a suitable low-Mg # end-member for sample TP6 that projects to Fo ~70.5 (Mg # ~41) at zero Ni. This could be derivate from crystallization or possibly a FeO and MgO-richer crustal partial melt [e.g., *Rapp and Watson*, 1995].

[22] Figure 12 also shows that the calculated paths of olivine fractionation are sometimes shallower than the observed trends in the high-Ni range (e.g., samples SPO60, TP10c). In fact, a considerable range in Ni at constant Fo is not compatible with fractional crystallization. A straightforward explanation is that this range reflects a range of Ni in the primary melts that may in turn be inherited from a mantle source that has a range of a few hundreds ppm Ni at a given Mg #. Alternatively, such vertical trends might also reflect magma mixing in a magma plumbing system that contained a broader variety of siliceous melt batches with different Mg # and Ni contents.

[23] In summary, the modeling results suggest that the Ni-rich olivines may mostly crystallize from partial melts that are derived from pyroxenite source lithologies. Low-Ni olivine may represent partial melts from either pyroxenite of peridotite. In addition, the overall variability is likely enhanced by preexisting source heterogeneity as well as additional processes of differentiation in the upper plate crust, such as magma mixing, and possibly some minor crustal assimilation.

4.3. Comparison to the *Sobolev et al.* [2005] Model

[24] The model outlined for the central MVB is based on the model of *Sobolev et al.* [2005]. However, some important details differ. In the Sobolev et al. model, partial melts added to peridotite carry Ca next to Si so that "reaction clinopyroxene" forms as well. The new pyroxenite

lithology then generates high-MgO melts (13.5–17 wt % MgO) that are unusually Ni-rich (700–1000 ppm) because of the low bulk D_{Ni} of ~1–1.17 in pyroxenite. In contrast, the MVB model does not need unusually Ni-rich mafic melts. The MVB model instead uses unusually low-MgO primary melts (~4–10 wt % MgO) with moderate Ni abundances (140–540 ppm Ni) that, after minor olivine fractionation, crystallize Ni-rich olivine because the olivine Kd_{Ni} is high (~12–37) in these melts (Figure 8). Moreover, there is no need for new clinopyroxene formation, which is consistent with the low mobility of Ca in slab fluids [e.g., *Kessel et al.*, 2004]. It is open to discussion whether such model-dependent contrasts may cause the strikingly different trends of central MVB olivines in the Ni versus Fo space (Figure 7) or whether additional factors relating to the different geotectonic setting are involved. The basic similarity of the models, however, points to the importance of such processes on a global scale independent of geotectonic setting.

5. Processing of the Subarc Mantle

5.1. Heterogeneity of the Subarc Mantle Source

[25] Figure 7 has already highlighted the conspicuous, subparallel trends of the central MVB olivines that cut through the fields of olivines from other geotectonic settings. Figure 12b shows that these trends are characteristic of individual samples. Samples with different Fo (or melt Mg #), but similar high-Ni olivines may erupt even from the same volcano (e.g., samples SPO60 and SPO56 from monogenetic volcano Cuatepel, Figure 12b). The importance of these trends is that they require a mantle source that is heterogeneous with respect to Mg #, because elements MgO, FeO and Ni must covary in cogenetic melts that mainly crystallize olivine. Since the process of pyroxenitization does not change the Mg # of mantle source, the source heterogeneity must be a characteristic of the peridotite mantle prior to pryroxenitization.

[26] A variable Mg # of peridotite mantle may be inherent, or it can be acquired by melting. Preexisting mantle heterogeneity is indicated by the mantle xenoliths from the Mexican Basin and Range Province which display a significant range in Mg #~89–91 at similar Ni = 2000 ± 200 ppm [*Heinrich and Besch*, 1992; *Luhr and Gomez-Aranda*, 1997; *Nimz et al.*, 1993]. With or without pyroxenitization, such mantle can produce melts with a range of Mg #, but similar Ni contents. On the other hand, the Mg # of mantle source can vary because of melting. This reflects the preferential partitioning of Fe into melt and the resultant decrease of the FeO/MgO in the residuum [e.g., *Langmuir et al.*, 1992]. Both melting modes (progressive melting of single source or serial melting) can create a significant range in Mg # and Ni in the source well prior the clinopyroxene exhaustion (Figure 9). Progressive melting, however, cannot decouple Ni from the FeO/MgO ratio of melt.

5.2. Evidence for Serial Melting

[27] While the preexisting source heterogeneity of the subarc mantle in the central MVB is elusive to assess, the possibility that the subarc mantle heterogeneity may be induced by melting is straightforward to test. This test uses the fact that the systematics of incompatible trace elements as well as that of MgO and FeO during mantle melting are well established [e.g., *Langmuir et al.*, 1992]. Consequently, if a melting link exists, the trends of these two groups must be in agreement. We focused on the samples that should be closest to primary melt compositions: those that have Ni-rich olivines (>1800 ppm Ni) and a calculated melt Ni of at least 100 ppm. The Mg # values of these samples were then combined with the trace elements of bulk rock.

[28] In subduction settings, incompatible trace elements are generally subdivided into two groups: first, the "mantle-controlled" elements (e.g., Nb, Ta, heavy REE) that are considered to reflect mantle processes, and second, the "slab-controlled" elements (e.g., fluid mobile LILE) that are dominated by slab contributions [e.g., *Pearce and Peate*, 1995; *Plank*, 2004; *Stolper and Newman*, 1994]. Earlier studies have already established that in the central MVB, the mantle-controlled elements and their ratios decrease systematically between alkaline to calc-alkaline end-members in ways consistent with depletion by melting [*LaGatta*, 2003; *Wallace and Carmichael*, 1999]. In contrast, the abundances of slab-controlled elements vary little, and hence the ratios of slab- to mantle-controlled elements (e.g., LILE/REE) increase rapidly with increasing source depletion (e.g., indicated by decreasing Nb, or Nb/Ta). In principle, this observation agrees with the concept that the amount of fluid added to the source is correlated with the extent of melting and hence with source depletion [e.g., *Stolper and Newman*, 1994]. *LaGatta* [2003] has already noted that the large range in Nb (~35 to ~5 ppm) is coupled with substantial decreases in

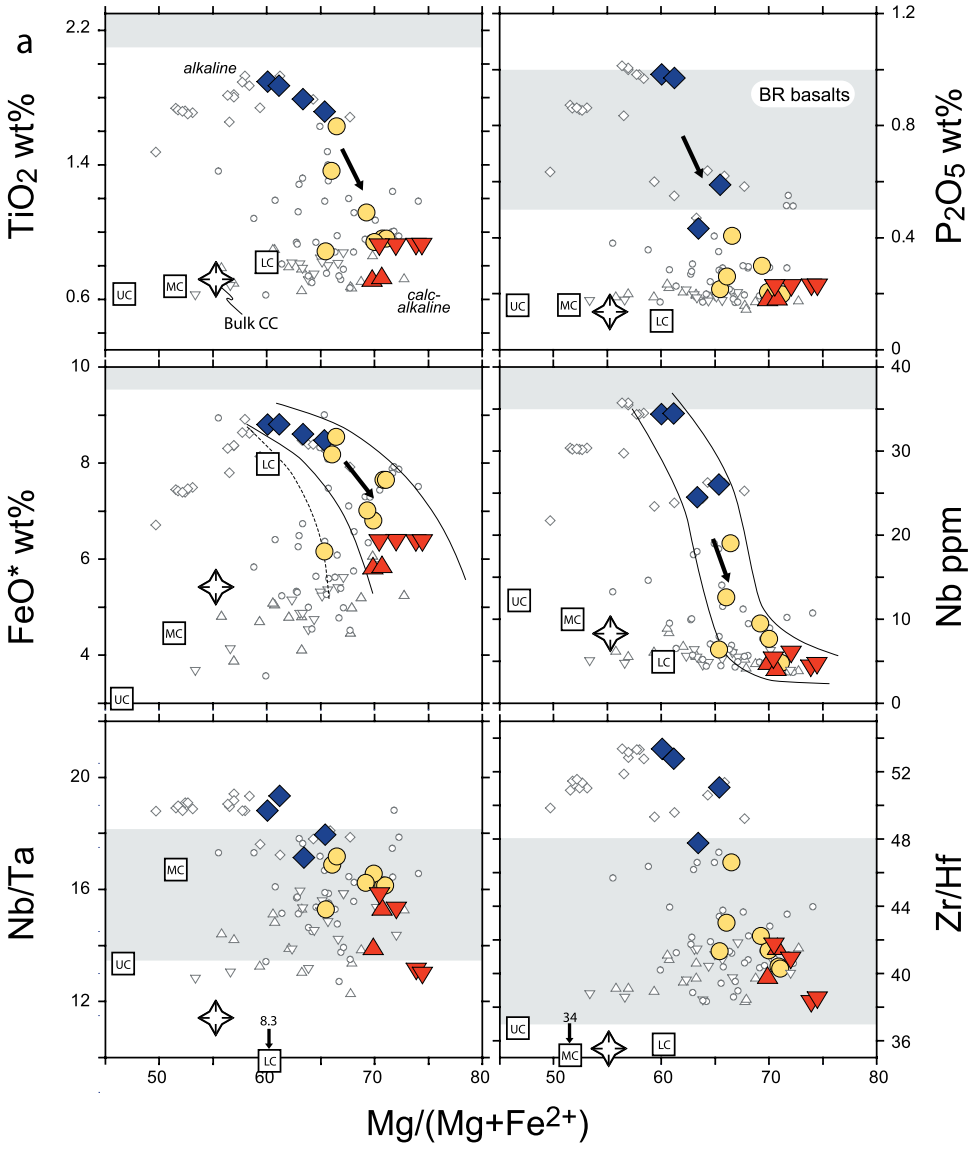

Figure 13. Mg $\#_{oliv}$ (Mg # calculated from average olivine per sample) versus selected abundances and ratios of trace and major elements of Ni-rich MVB andesites. (a) Examples of trends of "mantle-controlled" elements. (b) Examples of trends involving mobile, slab-derived elements (K, Na, and Pb). Symbols are as in Figure 1, but only samples with olivine Ni > 1800 ppm and calculated bulk Ni > 100 ppm are highlighted by colors. Other MVB samples are shown by smaller open symbols (data sources as in Figure 2). Analytical error (2σ) is within symbol sizes. Grey band indicates 2σ range of Mexican Basin and Range basalts (BR basalts). MORB (black circles) are after *Niu and Batiza* [1997]. Averages of continental crust (LC, lower crust; MC, middle crust; UC, upper crust; and star, bulk continental crust (CC)) are after *Rudnick and Gao* [2002]. Grey solid symbols show trends that K and Na would follow unless replenished by slab additions. See text for discussion.

Nb/Ta (~19 to ~14), Zr/Hf (~53 to ~38) and Nb/Yb (~9.5 to ~2.5). Such a range cannot be obtained by different extents of melting of a single source. Therefore *LaGatta* [2003] considered serial melting whereby each melting event in an increasingly depleted mantle was triggered by new fluid addition from the slab.

[29] Figure 13a confirms that similar strong correlations exist between the trace elements and their ratios, and the melt Mg #. The abundances and ratios of "mantle-controlled" incompatible elements in the near-primary melts correlate inversely with Mg $\#_{oliv}$ (Mg # of melt calculated from averaged olivine cores). These trends can readily be explained by progressive loss of clinopyroxene

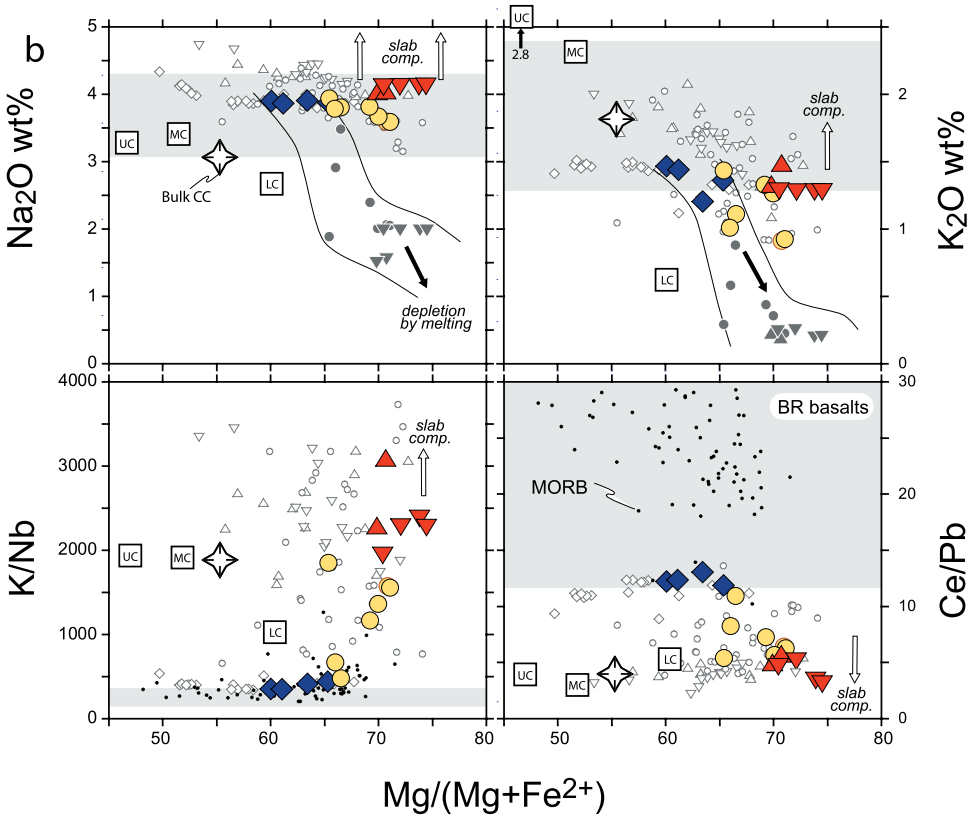

Figure 13. (continued)

from source that is the primary host of "mantle-controlled" trace elements (HFSE, HREE, Sc, V, >85% in fertile peridotite [*Eggins et al.*, 1998; *Witt-Eickschen and O'Neill*, 2005]). Published partition coefficients compiled by *Donnelly* [2002] and *LaGatta* [2003] indicate the following relative incompatibilities in clinopyroxene: $Kd_{Nb} < Kd_{Ta} \ll Kd_{Yb}$, and $Kd_{Zr} < Kd_{Hf}$ [*Green et al.*, 1989; *Hart and Dunn*, 1993; *Jenner et al.*, 1994; *Johnson*, 1994; *Salters and Longhi*, 1999; *Skulski et al.*, 1994]. As observed, this partitioning behavior predicts decreases of Nb, Nb/Ta and Zr/Hf with increasing source depletion (or Mg #).

[30] Unlike the "mantle-controlled" elements, the "slab-controlled" elements maintain high abundance levels, and are indifferent toward increasing Mg $\#_{oliv}$ (Figure 13b) Consequently, the LILE/HSFE and LILE/REE (e.g., K/Nb and Pb/Ce) ratios strongly increase with increasing Mg $\#_{oliv}$. These trends clearly exclude origin from a single, progressively melting source, but requires the addition of a slab component that balances the loss of these elements by melts. Importantly, a simple two-component mixing model across entire range is precluded with certainty owing to the subparallel trends these melts form in the Ni versus Fo diagram (Figure 12b). The only way to maintain steadily increasing LILE/HFSE ratios with increasing Mg # is then that melting must occur in many small events, i.e., serially. Each melting event should be connected to the addition of a slab component that impregnates the peridotite mantle, and partially transforms it into pyroxenite. As this process must eventually trigger melting, the continuous slab flux is thus the driving force of serial melting in the subarc mantle.

[31] The evidence of serial melting is further supported by quantitative considerations of Nb and Ta. Figure 14 shows a positive correlation of Nb with Nb/Ta of the near-primary central MVB melts (highlighted by colors). Qualitatively, the trend is consistent with the perception that alkaline and calc-alkaline end-member melt derive from enriched (high Nb) and depleted (low Nb) sources, respectively, and that these sources were related by melting. However, Nb and Ta are highly incompatible with very similar Kd in olivine, orthopyroxene and clinopyroxene, and hence are very

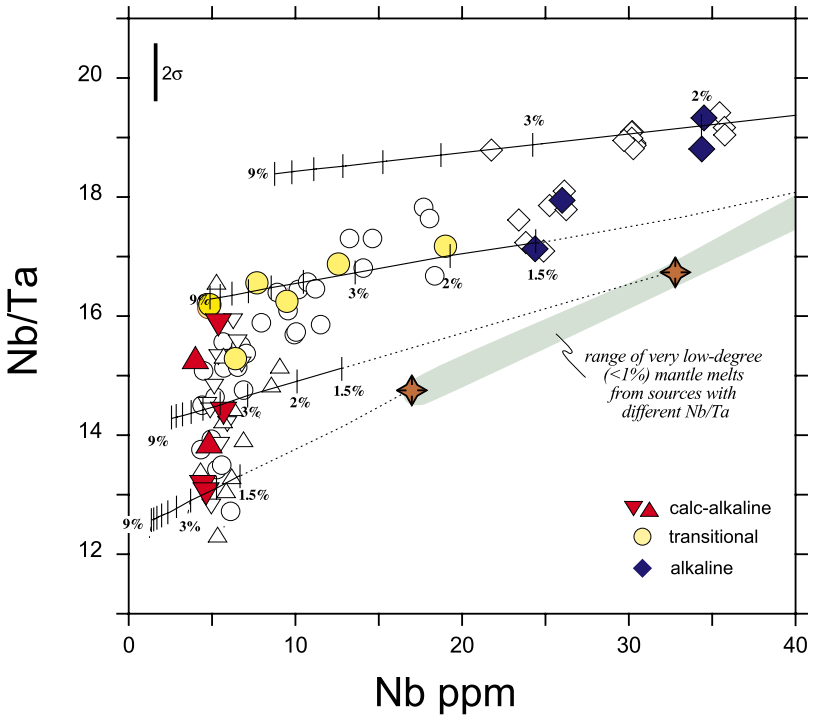

Figure 14. Nb versus Nb/Ta of bulk rocks. Symbols are as in Figure 1, but only samples with olivine Ni > 1800 ppm and calculated bulk Ni > 100 ppm are highlighted by colors. Two sigma bar indicates combined analytical error of Nb/Ta ratio. The four melting curves that emanate from a mantle heterogeneous with respect to Nb/Ta show the overall range of Nb/Ta in the central MVB cannot be produced by progressive melting of a single source. Tick marks indicate percentage of melting for up to 9%. Dotted lines extend melting curves back to very low degree melts (<1%) of mantle (green field). Stars approximate Nb/Ta of source. The Nb/Ta range of mantle source can be induced by serial melting, owing to the preferential partitioning of Nb into melt relative to Ta (D_{Nb}/D_{Ta} ~0.8). Four serial melting events with a total melt extraction of only ~1% are sufficient to produce the required Nb/Ta range of source (see also text). For the purpose of modeling a peridotite mantle was assumed (Oliv:Cpx:Opx:Grt = 56:23:19:2.2) as Nb and Ta should be mostly controlled by mantle clinopyroxene. Very similar results can be obtained for a pyroxenite source lithology. Starting source composition is Nb = 0.813 ppm, Ta = 0.0445 ppm (~primitive mantle), and Nb/Ta = 18.27. Mineral/melt partition coefficients are olivine Kd_{Nb} = 0.0015 and Kd_{Ta} = 0.0015, orthopyroxene Kd_{Nb} = 0.004 and Kd_{Ta} = 0.004, clinopyroxene Kd_{Nb} = 0.007 and Kd_{Ta} = 0.012; and garnet Kd_{Nb} = 0.03 and Kd_{Ta} = 0.04. Calculation uses nonmodal batch melting [*Shaw*, 1970] with melting reaction after *Longhi* [2002].

difficult to fractionate even at very low degrees of melting. Calculated melting curves of progressively melting, single mantle sources follow a much shallower slopes than the overall trend. The data array can only be reproduced when assuming a range of source compositions that have different Nb/Ta ratios (orange stars in green field in Figure 14). This range can be produced by serial melting, because the preferential removal of Nb from source effectively reduces the Nb/Ta in the residuum. Because of their very low Kd, Nb and Ta are so efficiently scavenged from the residue, that only a few percent total melt extraction (~1–2%) are required to generate a suitable range of Nb/Ta ratios in the source.

[32] This percentage of total melt loss, however, is considerably less than that suggested by the major element models which require up to ~20% total melt extraction from the same source. This contrast can be reconciled if Nb and Ta were not entirely "mantle-controlled," but became replenished from slab as well. The amount added would be minor relative to the "slab-controlled" elements, which is consistent with a strongly fractionated slab component with high LILE/REE and LILE/HFSE ratios [*Johnson and Plank*, 1999; *Kessel et al.*, 2004]. This concept agrees with *Gómez-Tuena et al.* [2007] who argued that water-rich silicate melts from slab added minor, but perceptible amounts of Nb and Ta with low Nb/Ta ratios (~10) that control low Nb/Ta ratios in MVB andesites west of Toluca volcano. Notably, minor slab additions of "mantle-controlled" elements at Toluca are also supported

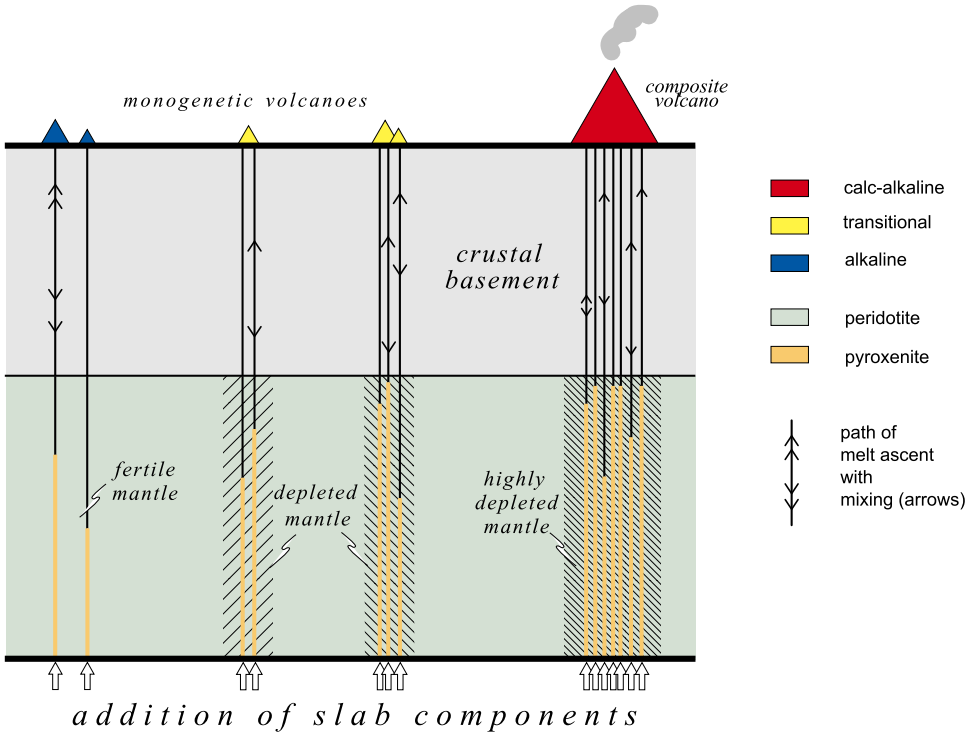

Figure 15. Cartoon depicting the melt generation model. For clarity the cartoon is restricted to Ni-rich near-primary melt compositions. See text for discussion.

by Nd and Hf isotope systematics [*Cai et al.*, 2007].

[33] In summary, the combined major and trace element systematics strongly support the role of serial melting in the evolution of the fertile mantle source of alkaline melts toward the depleted mantle source of calc-alkaline melts [*LaGatta*, 2003]. An important aspect of the model is that it depicts the subarc mantle as open system, where gain of material (from slab) and loss (by melting) are closely related in time and space.

6. A Working Model: Linking Slab Input to Pyroxenitization and Melting

[34] The cartoon in Figure 15 helps visualize the model proposed by relating the slab flux to pyroxenitization and melting. First, the slab component is added to the mantle. It provides the SiO_2 needed for pyroxenitization, but also adds H_2O and other fluid mobile LILE. Along vertical pathways, the peridotite transforms to pyroxenite where the newly formed reaction orthopyroxene acts a sink for the elements added from slab [e.g., *Liu et al.*, 2005]. Possibly, H_2O may be captured in transient hydrous phase (such as amphibole). Ambient mantle temperatures, that can be roughly estimated, are likely above >1200°C, the maximum temperature of olivine crystallization, but less than the anhydrous solidus for a given pressure (~1440°–1500°C [*Langmuir et al.*, 1992]). At these temperatures, the elements with high diffusivities and high abundances relative to the surrounding peridotite mantle (e.g., H_2O) will not stay confined in the pyroxenite, but will strive to equilibrate rapidly with the surrounding peridotite and lower its solidus. Melts from either lithology hybridize to primary basaltic andesite and andesite melts that are removed from source prior to refluxing of the residual source from slab.

[35] A key aspect of the MVB model is that it interprets each sample as single melt batch that has its own history of slab component infiltration, mantle pyroxenitization and melting. The infiltration of the subarc mantle apparently just started in the central Sierra Chichinautzin volcanic field where Ni-rich alkaline lavas with weak subduction signatures erupt (Figure 5). On the other hand, the process appears to be at its peak at Popo volcano where the subarc mantle has been extensively processed (and depleted) owing to frequent melting events. This inference also agrees with the erupted melt volumes that contrast strongly between the smaller, alkaline monogenetic centers (=1 km^3 [*Siebe et al.*, 2004b, 2005]) and Popocatepetl

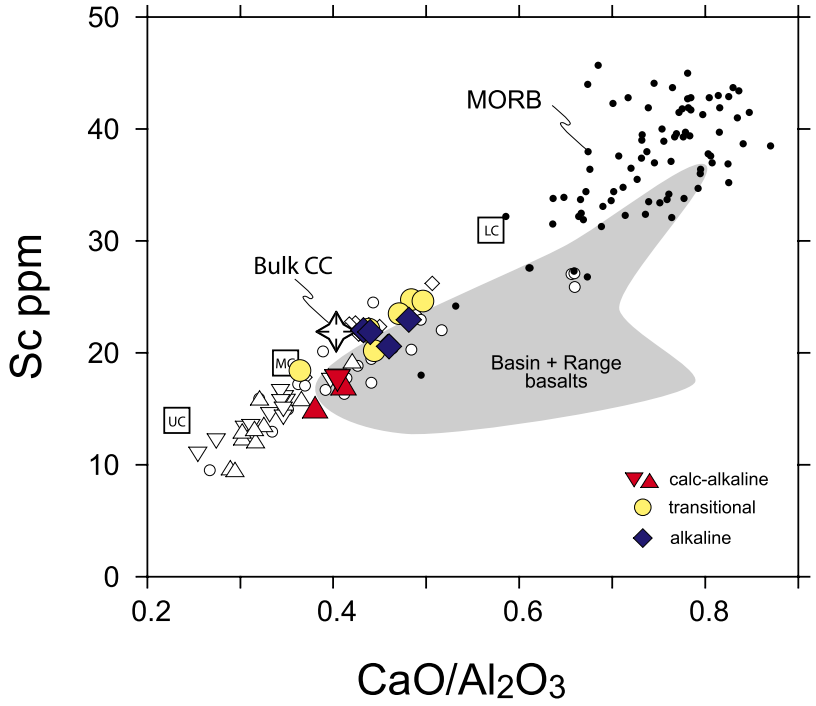

Figure 16. CaO/Al_2O_3 versus Sc (ppm) of Ni-rich central MVB andesites compared to Basin and Range basalts (grey field) and MORB. Data sources are Mexican Basin and Range basalts (as in Figure 2) and MORB [after *Niu and Batiza*, 1997]. Symbols are as in Figure 1, but only samples with olivine Ni > 1800 ppm and calculated bulk Ni > 100 ppm are highlighted by colors. Averages of continental crust are by *Rudnick and Gao* [2002].

volcano that has amassed about ~500 km^3 in countless eruptions during its estimated lifetime of several 100 ka [*Nixon et al.*, 1987; *Robin and Boudal*, 1987].

7. Creating Calc-Alkaline Andesites

[36] Last, we discuss the implications of the MVB model of melt formation for the major elements. Major elements are subject to the same laws as trace elements during melting and crystallization [*Langmuir et al.*, 1992] and their abundances in partial melts are equally dependent on source composition and on elemental partitioning behavior. This enables some conclusions based on the premise that the primitive Ni-rich melts are near-primary melts that have lost only little olivine.

[37] Major elements Ti, P, K and Na are incompatible during mantle melting, and minimally affected by minor olivine fractionation. Figure 13a shows that fluid immobile elements Ti and P behave similarly to other "mantle-controlled" trace elements, i.e., they decrease with increasing Mg $\#_{oliv}$. Therefore their conspicuous dearth in the calc-alkaline end-member melts is obviously due to depletion by serial melting. In contrast, fluid mobile elements Na and K are indifferent toward increasing Mg $\#_{oliv}$ which identifies them as added, "slab-controlled" elements. A slab contribution of K to calc-alkaline arc melts is commonplace [*Gill*, 1981], but the source of Na (slab versus mantle) is more controversial [e.g., *Langmuir et al.*, 2006; *Plank and Langmuir*, 1988; *Stolper and Newman*, 1994]. Notably, there is no discernible slab flux of Na and K to the fertile sources of alkaline end-member melts that may simply take in the slab flux. However, in order to maintain such high levels of K and Na with increasing source depletion, a substantial slab addition of K and Na is required. The amount added to the mantle sources of the Popo end-member can be estimated from mass balance, assuming trends that K and Na would follow if they were not replenished from slab. These projected "mantle trends" can be inferred by "mantle-controlled" elements that have similar Kd during melting and crystallization. Using Nb and Ti as proxies to K and Na, respectively, it shows that at least half of the K and Na in the erupted Popo melts must have been contributed from slab (Figure 13b).

[38] Major elements Ca, Si, Al, Fe, and Mg are less straightforward to interpret because they are (1) present in significant amounts in the mantle,

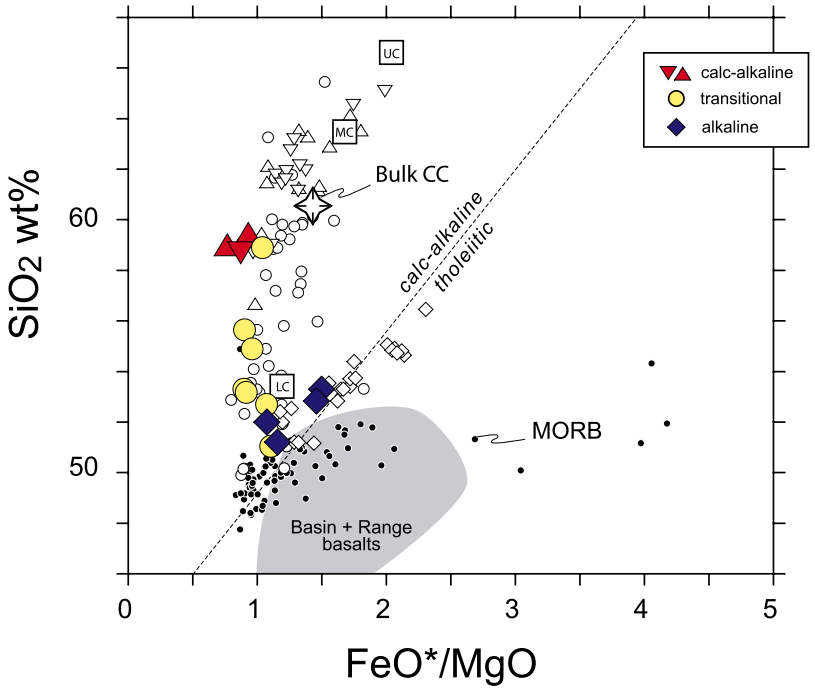

Figure 17. FeO/MgO versus SiO_2 (wt %) of Ni-rich central MVB lavas compared to Basin and Range basalts and MORB. Data sources and symbols as in Figure 16. Averages of continental crust are as in Figure 11. The line separating calc-alkaline from tholeiitic field is after *Miyashiro* [1974].

and (2) their partitioning behavior is a complex function of pressure, temperature and composition [*Langmuir et al.*, 1992]. However, some points can be made. First, silica must be added from the slab, because it is needed for orthopyroxene formation. In the Ni-rich primitive melts, silica increases from alkaline (~51 wt % SiO_2) to calc-alkaline (~60 wt % SiO_2) end-members. This increase would agree with a higher slab flux of SiO_2 to the calc-alkaline sources. On the other hand, SiO_2 may also significantly increase by hydrous melting [e.g., *Baker et al.*, 1994]. To distinguish among these influences, more measurements of primary meltwater contents are needed than are currently available for the central MVB [*Atlas et al.*, 2006; *Cervantes and Wallace*, 2003b]. Despite the uncertainty, however, the fact remains that the Si enrichment reflects slab and mantle processes, and is not due to differentiation in, or interaction with, the upper plate continental crust.

[39] Second, Figure 16 shows that the Ni-rich primitive melts possess the typical low CaO/Al_2O_3 (~0.4–0.5) of orogenic andesites which are distinct from MORB. Because minor olivine fractionation does not affect the CaO/Al_2O_3, the low CaO/Al_2O_3 should reflect a mantle signature, and not crustal processing. Notably, the low CaO/Al_2O_3 of the Ni-rich MVB melts is primarily a consequence of the lower CaO. While their Al_2O_3 abundances (~16.3 wt %) are close to the Basin and Range basalts (Al_2O_3 ~15 wt %) and MORB (Al_2O_3 ~15 wt %), their CaO abundances (~6.7 wt %) are much lower than Basin and Range basalts (~8.8 wt % CaO) and MORB (~9 wt % CaO). Low Ca may reflect low melting temperatures (and therefore high Kd_{Ca} in mantle clinopyroxene [*Langmuir et al.* [1992]), but also the progressive loss of clinopyroxene from the source. In contrast, some Al_2O_3 may even be added by slab fluids [e.g., *Kessel et al.*, 2004], which could maintain the abundance levels in a mantle subjected to serial melting.

[40] Finally, the "classical calc-alkaline trend of differentiation" i.e., the decrease of FeO with increasing SiO_2, Na_2O and K_2O can be identified as a mantle source characteristic (Figure 17). The consistently low FeO/MgO ratios (or high Mg #) of the Ni-rich melts apparently reflect buffering by a mantle that becomes depleted in FeO by melting. The control of FeO on the Mg # ratio is apparent as FeO decreases with increasing Mg # in the Ni-rich primitive melts (Figure 13a, from ~8 wt % in alkaline melts to ~5 wt % FeO in calc-alkaline melts) while the MgO is indifferent toward Mg #. This is exactly what one would predict from melts that form by serial melting from an increasingly

depleted source. Consequently, FeO cannot increase with increasing SiO_2, Na_2O or K_2O, but will decrease as the slab flux and the processes of the subarc mantle progress.

8. Comparison to Continental Crust

[41] If melt from mantle processed in subduction zones replicates the distinct major element signature of the continental crust, it is obvious that the Mg # of the near-primary melts of the central MVB melts are too high for average continental crust (Figure 13). In addition, the primitive melts of Mexico have higher ratios of Zr/Hf and Nb/Ta than average continental crust (Figure 13). While the latter discrepancy can be attributed to the enriched composition of the Mexican subarc mantle, the difference in Mg # by about ~15 units, suggests that additional differentiation processes are required to arrive at the lower Mg # of continental crust. However, creating the distinct major element fractionation of orogenic andesites by mantle processing in the first place emphasizes the role of the Earth's juvenile mantle in continental crust formation, as opposed to the recycling of preexisting crust [e.g., *Rudnick*, 1995].

Appendix A

A1. Samples and Methods

[42] The volcanic rock samples are typically fist-sized fragments of lavas flows, bombs or fallout tephra of impeccable origin. The samples were crushed, and hand-picked rock chips free from alteration were washed in triple-distilled water and methanol prior to powdering in an alumina mortar or an alumina shatter box. Major and trace elements of rock powders were determined by DCP (all major elements except P which was determined by ICP-MS at Harvard) and ICP-MS methods, respectively, either at Lamont (analyst: AB LaGatta) or at Harvard University (analyst: SM Straub). DCP analyses followed the methods reported by *Klein and Langmuir* [1987], whereby unknowns were calibrated with in-house standards MAR and K1919, and USGS standards BHVO-1 and BCR-1 (ABL at Lamont), and in-house standards MAR and LUM37, and USGS standards NBS688 and RGM1 (SMS at Harvard). ICP-MS analyses followed methods reported by *LaGatta* [2003], whereby unknown were calibrated by in-house standard MAR, USGS standards BHVO2 and BCR2 and GJS standard JB2 (Lamont and Harvard). Harvard analyses were monitored by repeat analyses of sample ASC1_S (from V. Chichinautzin). Standard deviation and RSD% are based on 5 analyses from different 4 digests for DCP analyses (April–September 2005), and 5 analyses from 8 different digests for ICP-MS (January to August 2005). Precision for DCP and ICPMS performed at Lamont is similar [*LaGatta*, 2003].

Table A1. Definitions

	Definition
K_d	mineral/melt partition coefficient
K_D	exchange coefficient between mineral and liquid (ratio of two partition coefficients) $K_{DFe2+-Mg}^{oliv/melt} = (Kd_{Fe}^{oliv/melt})/(Kd_{Mg}^{oliv/melt})$
D	bulk partition coefficient (melt/bulk rock)
C_o	concentration of element in source
C_L	concentration of element in liquid
Mg #	molar ratio of $Mg/(Mg+Fe^{2+})$ of bulk composition
Mg $\#_{oliv}$	molar ratio of $Mg/(Mg+Fe^{2+})$ calculated from olivine
P	pressure of melting
T	temperature of melting
γ	increment of melt produced per kbar (percent melt/kbar) (equals F)
F	increment of melt produced per kbar (equals γ)
F2	total amount of melt produced at a given P (equals $\Sigma\gamma$)

[43] Standard thin sections were prepared from most samples, and used to analyze olivine compositions for some samples. The majority of olivines analyzed were separated from bulk rock by crushing, magnetic separation (500–1000 μm fraction) and by handpicking. Except for the olivines from Popo's recent eruptions, all olivines were put into vertical gas mixing furnaces (DT-31-VT), using a CO_2-CO or CO_2-H_2 gas mixtures buffered near FMQ, at equilibration temperatures estimated from olivine bulk rock compositions after *Roeder and Emslie* [1970]. Under these conditions, glassy melt inclusions in olivines rehomogenized, while olivine composition is maintained [e.g., *Hauri*, 2002]. Olivine composition was preferentially measured close to primary melt inclusions. In recent eruption olivines, the olivine core region was targeted. Olivine data were collected by SMS between 1997 and 2004 at the Geomar/Germany (23% of data), at Lamont (69%) and the American Museum of Natural History in New York (8%) (Table 2). The olivine data from the Geomar are those discussed by *Straub and Martin-Del Pozzo* [2001], now fully published for the first time. Data were corrected for interlaboratory bias resulting from different calibration standards as described in

Table A2. Starting Composition of Peridotite Mantle Based on the Range of Mantle Xenoliths From the Mexican Basin and Range Province[a]

	Bulk MgO, wt %	Bulk FeO, wt %	Bulk Mg #	Bulk Ni, ppm	Ni in Olivine, ppm	Bulk K_2O, wt %	Bulk Na_2O, wt %	X_{CPX}[b]
Low-Mg # mantle	38.5	8.5	89	2200[c]	3100	0.03	0.27	16.5
High-Mg # mantle	44.0	7.8	91	1800[c]	2500	0.03	0.27	16.5

[a] See *Heinrich and Besch* [1992], *Luhr and Gomez-Aranda* [1997], and *Nimz et al.* [1993, 1995], and *Nimz et al.* [1993].
[b] Fraction of clinopyroxene in source.
[c] After dilution by slab components and transformation to pyroxenite, bulk Ni in source would be reduced to 1800 and 1500 ppm, respectively.

Table 3. Precision for SiO_2, FeO and MgO is around or better than 1% RSD. Typical precision for Ni is 3–5% RSD as determined from repeat analyses of San Carlos olivine (Table 3). Note that Ni abundances in olivine are given as Ni (and not NiO) to facilitate mineral/melt comparisons.

A2. Modeling Procedures

A2.1. Peridotite Melting

[44] Peridotite melting was modeled using the adiabatic decompression melting model of *Langmuir et al.* [1992]. This is a forward model that assumes the FeO and MgO concentration in peridotite melts to be constrained by residual olivine [*Hanson and Langmuir*, 1978; *Langmuir and Hanson*, 1980]. *Langmuir et al.* [1992] provide a set of equations for calculating the FeO and MgO abundances in liquid that take into account the dependency of their partition coefficients (Kd_{Mg} and Kd_{Fe}) on the pressure and temperature of melting, as well as the Na and K concentrations of the liquid. FeO and MgO variations with progressive melting can then be inferred by combining these data with a "melting function," which provides temperature and the extent of melting for a given pressure of melting. The model needs few input parameters: Mg, Fe, Na and K of bulk source (mantle peridotite), the pressure of melting, and fraction of clinopyroxene in source. The equations are discussed in detail by *Langmuir et al.* [1992], and only the essential steps are reiterated here. Definition and acronyms of terms are given in Table A1. Mantle source compositions are listed in Table A2, and all other parameters are summarized in Table A3.

A2.2. Choice of Peridotite Bulk Compositions and Pressure of Melting

[45] The peridotite bulk compositions in Table A2 are based on analyses of mantle xenoliths from Quaternary tuff cones in the Mexican Basin and

Table A3. Input Parameters for Mantle Melting Model

Parameter	Numerical Value and/or Unit	Definition
P (initial pressure of melting)	2.2 GPa (~73 km)	
$K_{Doliv/liq}^{Fe/Mg}$	0.295	
$K_{Dopx/liq}^{Fe/Mg}$	0.255	
D_{K2O} (peridotite melting)	0.005	
H_f	180 cal gm^{-1}	heat of fusion
C_P	0.3 cal gm^{-1} deg^{-1}	heat capacity
dT/dP_{adb}	1° $kbar^{-1}$	slope of adiabat
dT/dP_{sol}	13° $kbar^{-1}$	slope of solidus
dT/dF	6°C per percent of melting for portion below 22% melting, 8°C per percent melting for portion above 22% melting	temperature change above solidus needed to melt a given amount peridotite mantle
X_{cpx}	16.5%	fraction of clinopyroxene in peridotite mantle

Range province [*Heinrich and Besch*, 1992; *Luhr and Gomez-Aranda*, 1997; *Nimz et al.*, 1993, 1995]. These xenoliths represent the upper mantle beneath the North American plate and compare well to any other upper mantle xenoliths. Ni abundance in olivine is based on the average Ni content in the olivines of these xenoliths, which include olivine data from arc front xenoliths [*Blatter and Carmichael*, 1998a]. The range of Ni in olivine (2500–3100 ppm) used in modeling represents one standard deviation above and below the average (Ni = 2800 ± 300 ppm). The corresponding Ni in bulk source is 1800–2200 ppm Ni. The initial pressure of melting was set at 2.2 GPa (~73 km) in the middle of the mantle wedge and a decrease of 0.05 GPa per melt increment was assumed. Overall, the model is fairly insensitive toward any reasonable starting pressure and pressure gradients.

A2.3. Melting Program

[46] The parameter γ (= change in melt fraction with change in pressure above the solidus) is calculated as function of heat of fusion, heat capacity, slope of adiabat, slope of solidus and dT/dF:

$$\gamma = (dT/dP_{ad} - dT/dP_{sol})/(H_f/C_P + dT/dF * (1 - P/88))$$

whereby (1-P/88) is a pressure correction on the melting contours. The value of γ is 1.14% kbar^{-1} for the first increments of melting, and decreases during progressive melting to about 1% kbar^{-1} at an extent of melting ~20%. The variable γ equals the increment of melt (F) produced per step of melting, while the total amount of melt (F2) at a given pressure of melting is the sum of all melt increments.

[47] The melting temperature for a given pressure can then be calculated as function of the dT/dF and a correction for source heterogeneity:

$$T(\text{in } ^\circ C) = 1150 + 13 * P + dT/dF * F2 * (1 - P/88) + 20 * (Mg\ \#_{source} - 89)$$

[48] The first term of the equation uses the experimentally determined solidus temperatures (after *McKenzie and Bickle* [1988], as discussed by *Langmuir et al.* [1992]). The second term accounts for the temperature change above solidus that is needed to melt the total amount of melt (including a pressure correction). The third term accounts for source heterogeneity, assuming that the mantle solidus increases by 20°C for each unit increase in Mg #. For an extent of melting <22%, the value of dT/dF is 6°C per percent melting, and above >22%, the value of dT/dF is 8°C per percent melting. The change of dT/dF is effected by the disappearance of clinopyroxene from source.

[49] If F is known, Na_2O and K_2O of equilibrium liquids can be calculated from their source abundances and the percentage of clinopyroxene in source (Table A3):

$$C_L/C_o = 1/(F1 + D * (1 - F1))$$

whereby D_{K2O} is assumed to be constant (= 0.005, Table A3). D_{Na2O} is calculated as a function of P, T and X_{CPX} in source:

$$D_{Na2O} = a + 10^{((b+c*P)/(T+273)-d)} * X_{CPX} * e$$

whereby a, b, c, d and e are constants.

[50] The Kd_{Mg} and Kd_{Fe} are then calculated for the appropriate temperatures and pressures:

$$\ln Kd_{Mg} = a/(273 + T) + b * X_{Na} + c * K_2O + d * P - e$$

whereby a, b, c, d and e are constants.

$$Kd_{Fe} = 0.295 * Kd_{Mg}$$

whereby K_2O is K_2O in liquid, and X_{Na} is cation fraction of Na_2O in liquid.

[51] If olivine controls the MgO and FeO in liquid, the liquid concentration of MgO and FeO are then calculated by

$$XMg_{liq} = XMg_{oliv}/Kd_{Mg}$$

$$XFe^{tot}_{liq} = XFe_{oliv}/Kd_{Fe}$$

whereby XMg and XFe are the cation mole% of MgO and FeO in melt and olivine respectively.

[52] The melting program models progressive melting (increasing extent of melting of a single source) for an extent of melting of up to 35%, as well as serial melting (repetitive extraction of small-degree melts extraction from a single source). The latter is possible, since the program creates melt incrementally in approximately 1% melt fractions. Thus the residual source composition of Mg, Fe, Na, and K can be calculated by mass balance for each increment. The fraction of residual X_{CPX} can be calculated, assuming that clinopyroxene contributes 60% to the liquid produced per increment of melting. In this study, serial melting was performed in arbitrarily chosen 2%

steps. In either melting mode (progressive or serial), clinopyroxene would be exhausted after ~20–22% melting. Serial melting is similar to fractional melting, except, as it is argued, that the system is not closed, as each melting step is considered to be triggered by addition of a slab component.

A2.4. Ni in Liquid and Olivine

[53] The *Langmuir et al.* [1992] melting model was extended to allow modeling of Ni concentrations in liquid and residual peridotite. Most of the mantle Ni (~80–90%) is stored in olivine, which is the most abundant mantle mineral with the highest Kd_{Ni} among all mantle minerals at any given Kd_{Mg} [e.g., *Beattie et al.*, 1991] (Figure 8). Therefore Ni concentrations in liquid and residual will be controlled by olivine. Several experimental calibrations provide a quantitative description of the olivine Kd_{Ni} as function of either olivine Kd_{Mg}, or melt MgO [*Beattie et al.*, 1991; *Hart and Davis*, 1978; *Kinzler et al.*, 1990]. These equations all provide very similar results of the Kd_{Ni} for peridotite melting as well as for olivine crystallization from peridotite melts.

[54] The olivine Kd_{Ni} for peridotite melting and olivine crystallization was calculated using the melt MgO of peridotite melts and the equation of *Hart and Davis* [1978]. The Kd_{Ni} allows for inferring melt Ni if the Ni content of olivine is known for each increment of melts. Using a range of starting compositions of 2500 to 3100 ppm Ni in olivine, the Ni content of the residual olivine per melt increment is calculated by mass balance.

A2.5. Pyroxenite Melting

[55] No quantitative model for pyroxenite melting exists. Pyroxenite formation results from the elimination of olivine in source, at least to the point where olivine does not control melt content of Mg, Fe and Ni anymore. Instead, these elements should be now controlled by orthopyroxene that is their main host and that dominates the source lithology. The influence of clinopyroxene on melt Mg, Fe and Ni is negligible, although clinopyroxene does control Ti, P and many other "mantle-controlled" trace elements (e.g., REE). If neither Mg nor Fe are added or lost during the reaction transformation, then the "reaction orthopyroxene" must inherit the Mg # of the olivine destroyed. Because the orthopyroxene $K_D^{Fe-Mg} = 0.255$ is only slightly lower than that of the olivine $K_D^{Fe-Mg} = 0.295$, the Mg # of partial melt is only slightly lower than those of peridotite melts. Ni is more variable. For one, Ni is diluted by the silica addition. Assuming 55–80% fosteritic olivine in bulk peridotite, 14–20% of silica are needed to transform all olivine to orthopyroxene based on the stochiometric reaction (SiO_2 + $(Mg, Fe, Mg)_2SiO_4 = (Mg, Fe)_2Si_2O_6$). Thus the Ni of bulk source (~1800–2200 ppm) is lowered to ~1500–1800 ppm Ni. To the other, the orthopyroxene Kd_{Ni} is ~3 times lower than the olivine Kd_{Ni} (Figure 8). Therefore the Ni content of the partial melts from pyroxenite is similar to those from peridotite melts. Because of the low bulk melt MgO (~4–10 wt %) of pyroxenite melts, high-Ni olivines will crystallize at shallow pressures.

[56] Consequently, the field for low-MgO pyroxene melts must be located somewhere above and slightly to the left of the field of peridotite melts in the Ni versus Fo diagram (Figure 12). To calculate this field, the Mg # of the peridotite source were taken to be those of orthopyroxene. The Mg # of equilibrium melts can then be calculated using the exchange coefficient $K_D^{Fe-Mg} = 0.255$. Assuming a MgO value for this melt (here 4 or 10 wt % MgO), the melt FeO is constrained. Assuming a bulk Ni content of pyroxenite in source, these data allow then for calculating MgO of orthopyroxene and the Ni melt using the orthopyroxene Kd_{Ni} of *Beattie et al.* [1991]. The bulk Ni of the pyroxenite source (~1500–1800 ppm) was taken to be that bulk peridotite source (~1800–2200 ppm) after dilution by the slab component. Using the olivine Kd_{Ni} of *Beattie et al.* [1991], the Ni contents of olivine in equilibrium can then be calculated for the appropriate melt MgO.

Acknowledgments

[57] This study was supported by the "Deutsche Forschungsgemeinschaft" by research fellowships STR 441/4 and 441/6 to S.M.S. and U.S. National Science Foundation grant EAR 96-14782 to C.H.L. and S. L. Goldstein that supported the Ph.D. thesis of A.B.L. Ramon Espinasa-Perena contributed greatly to the successful fieldwork. Dave Walker was an invaluable source of wisdom, advice, and support. He also enabled the electron microprobe work at Lamont. We thank Dave Walker, Arturo Gomez-Tuena, and Georg Zellmer for inspiring discussions and insightful comments and Charlie Mandeville and Sue Woods for help in the lab. The manuscript benefited substantially from reviews by Alex Sobolev, Paul Wallace, and Zhengrong Wang as well as additional comments and the editorial work of Glenn Gaetani and Vincent Salters.

References

Atlas, Z. D., J. E. Dixon, G. Sen, M. Finny, and A. L. Martin-Del Pozzo (2006), Melt inclusions from Volcan Popocatepetl and Volcan de Colima, Mexico: Melt evolution due to vapor-

saturated crystallization during ascent, *J. Volcanol. Geotherm. Res.*, *153*, 221–240.
Baker, M. B., T. L. Grove, and R. Price (1994), Primitive basalts and andesites from the Mt. Shasta region, N. California: Products of varying melt fraction and water content, *Contrib. Mineral. Petrol.*, *118*, 111–129.
Beard, J. S., and G. E. Lofgren (1991), Dehydration melting and water-saturated melting of basaltic and andesitic greenstones and amphibolites at 1, 3 and 6.9 kbar, *J. Petrol.*, *32*(2), 365–401.
Beattie, P., C. Ford, and D. Russell (1991), Partition coefficients for olivine-melt and orthopyroxene-melt systems, *Contrib. Mineral. Petrol.*, *109*, 212–224.
Blatter, D. L., and I. S. E. Carmichael (1998a), Hornblende peridotites xenoliths from central Mexico reveal the highly oxidized nature of the subarc upper mantle, *Geology*, *26*(11), 1035–1083.
Blatter, D. L., and I. S. E. Carmichael (1998b), Plagioclase-free andesites from Zitacuaro (Michoacan), Mexico: Petrology and experimental constraints, *Contrib. Mineral. Petrol.*, *132*, 121–138.
Blatter, D. L., and I. S. E. Carmichael (2001), Hydrous phases equilibria of a Mexican high-silica andesite: A candidate for a mantle origin?, *Geochim. Cosmochim. Acta*, *65*, 4043–4065.
Cai, Y. M., et al. (2007), Subduction contributions in the Trans-Mexican Volcanic Belt: Implications from lava chemistry and Hf-Nd-Pb isotopes, *Eos Trans. AGU*, *88*(23), Jt. Assem. Suppl., Abstract V52A-03.
Carmichael, I. S. E. (2002), The andesite aqueduct: Perspectives on the evolution of intermediate magmatism in west-central (105–99°W) Mexico, *Contrib. Mineral. Petrol.*, *143*, 641–663.
Cervantes, P., and P. J. Wallace (2003a), Magma degassing and basaltic eruption styles: A case study of ~2000 year BP Xitle volcano in central Mexico, *J. Volcanol. Geotherm. Res.*, *120*, 249–270.
Cervantes, P., and P. Wallace (2003b), The role of H_2O in subduction zone magmatism: New insights from melt inclusions in high-Mg basalts from central Mexico, *Geology*, *31*(3), 235–238.
Chesley, J., J. Ruiz, K. Righter, L. Ferrari, and A. Gomez-Tuena (2002), Source contamination versus assimilation: An example from the Trans-Mexican Volcanic Arc, *Earth Planet. Sci. Lett.*, *195*, 211–221.
Clynne, M. A., and L. E. Borg (1997), Olivine and chromian spinel in primitive calc-alkaline and tholeiitic lavas from the southernmost Cascade Range, California: A reflection of relative fertility of the source, *Can. Mineral.*, *35*, 453–472.
Davidson, J. P. (1987), Crustal contamination versus subduction zone enrichment: Examples from the Lesser Antilles and implications for mantle source compositions of island arc volcanic rocks, *Geochim. Cosmochim. Acta*, *51*, 2185–2198.
Defant, M., and M. Drummond (1990), Derivation of some modern arc magmas by melting of young subducted lithosphere, *Nature*, *347*, 662–665.
Donnelly, K. E. (2002), The genesis of MORB: Extensions and limitations of the hot spot model, Ph.D. thesis, Columbia Univ., New York.
Eggins, S. M., R. L. Rudnick, and W. F. McDonough (1998), The composition of peridotites and their minerals: A laser-ablation ICP-MS study, *Earth Planet. Sci. Lett.*, *154*, 53–71.
Ertan, I. E., and W. P. Leeman (1996), Metasomatism of Cascades subarc mantle: Evidence from a rare phlogopite orthopyroxenite xenolith, *Geology*, *24*(5), 451–454.
Ewart, A., and W. L. Griffin (1994), Application of proton-microprobe data to trace element partitioning on volcanic rocks, *Chem. Geol.*, *117*, 251–284.
Falloon, T. J., L. V. Danyushevsky, A. Ariskin, D. H. Green, and C. E. Ford (2007), The application of olivine geothermometry to infer crystallization temperatures of parental liquids: Implications for the temperature of MORB magmas, *Chem. Geol.*, *241*, 207–233.
Gill, J. (1981), *Orogenic Andesites and Plate Tectonics*, 390 pp., Springer, New York.
Gómez-Tuena, A., A. B. LaGatta, C. H. Langmuir, S. L. Goldstein, F. Ortega-Gutiérrez, and G. Carrasco-Núñez (2003), Temporal control of subduction magmatism in the eastern Trans-Mexican Volcanic Belt: Mantle sources, slab contributions, and crustal contamination, *Geochem. Geophys. Geosyst.*, *4*(8), 8912, doi:10.1029/2003GC000524.
Gómez-Tuena, A., T. M. Orozco-Esquivel, and L. Ferrari (2006), Petrogenesis ignea de la Faja Volcanica Transmexicana, in *Volumen Conmemorativo del Centenario: Temos selectos de la Geologia Mexicana*, edited by S. Alaniz, *Bol. Soc. Geol. Mex.*, *LVII*, 229–287.
Gómez-Tuena, A., C. H. Langmuir, S. L. Goldstein, S. M. Straub, and F. Ortega-Gutierrez (2007), Geochemical evidence for slab melting in the Trans-Mexican Volcanic Belt, *J. Petrol.*, *48*(3), 537–562, doi:10.1093/petrology/egl071.
Green, T. H., S. H. Sie, C. Ryan, and D. Cousens (1989), Proton microprobe-determined partitioning of Nb, Ta, Zr, Sr and Y between garnet, clinopyroxene and basaltic magma at high-pressure and temperature, *Chem. Geol.*, *74*, 201–216.
Hanson, G. N., and C. H. Langmuir (1978), Modelling of major elements in mantle-melt systems using trace element approaches, *Geochim. Cosmochim. Acta*, *42*, 725–741.
Hart, S. R., and K. E. Davis (1978), Nickel partitioning between olivine and silicate melt, *Earth Planet. Sci. Lett.*, *40*, 203–219.
Hart, S. R., and T. Dunn (1993), Experimental cpx/melt partitioning of 24 trace elements, *Contrib. Mineral. Petrol.*, *113*, 1–8.
Hauri, E. (2002), SIMS analysis of volatiles in silicate glasses, 2. Isotopes and abundances in Hawaiian melt inclusions, *Chem. Geol.*, *183*, 115–142.
Heinrich, W., and T. Besch (1992), Thermal history of the upper mantle beneath a young back-arc extensional zone: Ultramafic xenoliths from San Luis Potosi, central Mexico, *Contrib. Mineral. Petrol.*, *111*, 126–142.
Hildreth, W., and S. Moorbath (1988), Crustal contributions to arc magmatism in the Andes of central Chile, *Contrib. Mineral. Petrol.*, *98*, 455–489.
Hirschmann, M. M., and E. M. Stolper (1996), A possible role for garnet pyroxenite of the origin of the 'garnet signature' in MORB, *Contrib. Mineral. Petrol.*, *124*, 185–208.
Hirschmann, M., T. Kogiso, and M. Pertermann (2006), Petrologic considerations of pyroxenite heterogeneities in basalt source regions, paper presented at Fifth GERM Workshop, Lamont-Doherty Earth Obs., The Earth Inst. at Columbia Univ., New York.
Jenner, G., et al. (1994), Determination of partition coefficients for trace elements in high pressure-temperature experimental run products by laser-ablation microprobe-inductively coupled plasma-mass spectrometry (LAM-ICP-MS), *Geochim. Cosmochim. Acta*, *57*, 5099–5103.
Johnson, K. T. M. (1994), Experimental cpx/melt and garnet/melt partitioning of REE and other trace elements at high pressure: Petrogenetic implications, *Mineral. Mag.*, *58A*, 454–455.
Johnson, M. C., and T. Plank (1999), Dehydration and melting experiments constrain the fate of subducted sediments, *Geochem. Geophys. Geosyst.*, *1*(1), doi:10.1029/1999GC000014.

Kay, R. W. (1978), Aleutian magnesian andesites: Melts from subducted Pacific Ocean crust, *J. Volcanol. Geotherm. Res.*, *4*, 117–132.

Kelemen, P. B. (1995), Genesis of high Mg# andesites and the continental crust, *Contrib. Mineral. Petrol.*, *120*, 1–19.

Kelemen, P. B., S. R. Hart, and S. Bernstein (1998), Silica enrichment in the continental upper mantle via melt/rock reaction, *Earth Planet. Sci. Lett.*, *164*, 387–406.

Kelemen, P. B., K. Hanghoi, and A. R. Greene (2004), One view of the geochemistry of subduction-related magmatic arcs, with an emphasis on primitive andesite and lower crust, in *Treatise on Geochemistry*, vol. 3, *The Crust*, edited by R. L. Rudnick, pp. 593–659, Elsevier, New York.

Kessel, R., P. Ulmer, T. Pettke, M. W. Schmidt, and A. B. Thompson (2004), A novel approach to determine high-pressure high-temperature fluid and melt compositions using diamond-trap experiments, *Am. Mineral.*, *89*, 1078–1086.

Kilinc, A., I. S. E. Carmichael, M. L. Rivers, and R. O. Sack (1983), The ferric-ferrous ratio of natural silicate liquids equilibrated in air, *Contrib. Mineral. Petrol.*, *83*, 136–140.

Kinzler, R. J., T. L. Grove, and S. I. Recca (1990), An experimental study on the effect of temperature and melt composition on the partitioning of nickel between olivine and silicate melt, *Geochim. Cosmochim. Acta*, *54*, 1255–1265.

Klein, E. M., and C. H. Langmuir (1987), Global correlations of ocean ridge basalt chemistry with axial depth and crustal thickness, *J. Geophys. Res.*, *92*(B8), 8089–8115.

Kogiso, T., M. Hirschmann, and M. Pertermann (2004), High-pressure partial melting of mafic lithologies in the mantle, *J. Petrol.*, *45*(12), 2407–2422, doi:101093/petrology/egh057.

LaGatta, A. B. (2003), Arc magma genesis in the eastern Mexican volcanic belt, Ph.D. thesis, 329 pp., Columbia Univ., New York.

Langmuir, C. H., and G. N. Hanson (1980), An evaluation of major element heterogeneity in the mantle sources of basalts, *Philos. Trans. R. Soc. London, Ser. A*, *297*, 383–407.

Langmuir, C. H., E. M. Klein, and T. Plank (1992), Petrological systematics of mid-ocean ridge basalts: Constraints on melt generation beneath ocean ridges, in *Mantle Flow and Melt Generation at Mid-Ocean Ridges*, *Geophys. Monogr. Ser.*, vol. 71, edited by J. P. Morgan, D. K. Blackman, and J. M. Sinton, pp. 183–280, AGU, Washington, D. C.

Langmuir, C. H., A. Bezos, S. Escrig, and S. W. Parman (2006), Chemical systematics and hydrous melting of the mantle in back-arc basins, in *Back-Arc Spreading Systems—Geological, Biological, Chemical, and Physical Interactions*, *Geophys. Monogr. Ser.*, vol. 166, edited by D. M. Christie et al., pp. 87–146, AGU, Washington, D. C.

Lawlor, P. J., et al. (1999), U-Pb geochronology, geochemistry, and provenance of the Grenvillian Huiznopala gneiss of eastern Mexico, *Precambrian Res.*, *94*, 73–99.

Leeman, W. P., and D. J. Lindstrom (1978), Partitioning of Ni^{2+} between basaltic melts and olivines—An experimental study, *Geochim. Cosmochim. Acta*, *42*, 801–816.

Leeman, W. P., and K. F. Scheidegger (1977), Olivine/liquid distribution coefficients and a test for crystal-liquid equilibrium, *Earth Planet. Sci. Lett.*, *35*, 247–257.

Leeman, W. P., J. F. Lewis, R. C. Evarts, R. M. Conrey, and M. J. Streck (2005), Petrologic constraints on the thermal structure of the Cascades arc, *J. Volcanol. Geotherm. Res.*, *140*, 67–105.

Li, C., E. M. Ripley, and E. A. Mathez (2003), The effect of S on the partitioning of Ni between olivine and silicate melt in MORB, *Chem. Geol.*, *201*, 295–306.

Liu, Y., et al. (2005), Melt-peridotite interactions: Links between garnet pyroxenite and high-Mg# signature of continental crust, *Earth Planet. Sci. Lett.*, *234*, 39–57.

Longhi, J. (2002), Some phase equilibrium systematics of lherzolite melting: I, *Geochem. Geophys. Geosyst.*, *3*(3), 1020, doi:10.1029/2001GC000204.

Luhr, J. F. (1997), Extensional tectonics and the diverse primitive volcanic rocks in the western Mexican Volcanic Belt, *Can. Mineral.*, *35*, 473–500.

Luhr, J. F., and J. J. Gomez-Aranda (1997), Mexican peridotite xenoliths and tectonic terranes: Correlations among vent location, texture, temperature, pressure and oxygen fugacity, *J. Petrol.*, *38*(8), 1075–1112.

Luhr, J. F., J. J. Aranda-Gomez, and J. G. Pier (1989), Spinel-lherzolithe-bearing Quaternary volcanic centers in San Luis Potosí, Mexico: 1. Geology, mineralogy, and petrology, *J. Geophys. Res.*, *94*(B6), 7916–7940.

Luhr, J. F., J. G. Pier, J. J. Aranda-Gomez, and F. A. Posedek (1995a), Crustal contamination in early Basin-and-Range hawaiites of the Los Encinos volcanic field, central Mexico, *Contrib. Mineral. Petrol.*, *118*, 321–339.

Luhr, J. F., J. J. Aranda-Gomez, and T. Housh (1995b), San Quintin volcanic field, Baja California Norte, Mexico: Geology, petrology, and geochemistry, *J. Geophys. Res.*, *100*(B7), 10,353–10,380.

Manea, V. C., M. Manea, V. Kostoglodov, C. A. Currie, and G. Sewell (2004), Thermal structure, coupling and metamorphism in the Mexican subduction zone beneath Guerrero, *Geophys. J. Int.*, *158*, 775–784.

Martinez-Serrano, R. G., et al. (2004), Sr, Nd and Pb isotope and geochemical data from the Quaternary Nevado the Toluca volcano, a source of recent adakite magmatism, and the Tenango volcanic field, *J. Volcanol. Geotherm. Res.*, *138*, 77–110.

Maurel, C., and P. Maurel (1982), Etude experimentale de l'equilibire Fe2+-Fe3+ dans les spinelles chromiferes et les liquides silicates basiques, a 1 atm, *C. R. Acad. Sci. Paris, Ser. II*, *295*, 209–212.

McKenzie, D. P., and M. J. Bickle (1988), The volume and composition of melt generated by extension of the lithosphere, *J. Petrol.*, *29*(3), 625–679.

Miyashiro, A. (1974), Volcanic rock series in island arcs and active continental margins, *Am. J. Sci.*, *274*, 321–355.

Morris, J. D., W. P. Leeman, and F. Tera (1990), The subducted component in island arc lavas: Constraints from Be isotopes and B-Be systematics, *Nature*, *344*, 31–36.

Nimz, G. J., K. L. Cameron, and S. Niermayer (1993), The La Olivina pyroxenite suite and the isotopic compositions of mantle basalts parental to the mid-Cenozoic arc volcanism of northern Mexico, *J. Geophys. Res.*, *98*(B4), 6489–6509.

Nimz, G. J., K. I. Cameron, and S. Niermayer (1995), Formation of mantle lithosphere beneath northern Mexico: Chemical and Sr-Nd-Pb isotopic systematics of peridotite xenoliths from La Olivina, *J. Geophys. Res.*, *100*(B3), 4181–4196.

Niu, Y., and R. Batiza (1997), Trace element evidence from seamounts for recycled oceanic crust in the eastern Pacific mantle, *Earth Planet. Sci. Lett.*, *148*, 471–483.

Nixon, G. T. (1988a), Petrology of the younger andesites and dacites of Iztaccihuatl Volcano, Mexico: I. Disequilibrium phenocryst assemblages as indicators of magma chamber processes, *J. Petrol.*, *29*(2), 213–264.

Nixon, G. T. (1988b), Petrology of the younger andesites and dacites of Iztaccihuatl Volcano, Mexico: II. Chemical stratigraphy, magma mixing, and the composition of basaltic magma influx, *J. Petrol.*, *29*(2), 265–303.

Nixon, G. T., A. Demant, R. L. Armstrong, and J. E. Harakal (1987), K-Ar and geological data bearing on the age and evolution of the Trans-Mexican Volcanic Belt, *Geofis. Int.*, *26*(1), 109–158.

Pearce, J. A., and D. W. Peate (1995), Tectonic implications of the compositions of volcanic arc magmas, *Annu. Rev. Earth Planet. Sci.*, *23*, 251–285.

Pier, J. G., F. A. Podosek, J. F. Luhr, and J. C. Brannon (1989), Spinel-lherzolite-bearing Quaternary volcanic centers in San Luis Potosi, Mexico: 2. Sr and Nd isotopic systematics, *J. Geophys. Res.*, *94*(B6), 7941–7951.

Plank, T. (2004), Constraints from thorium/lanthanum on sediment recycling at subduction zones and the evolution of the continents, *J. Petrol.*, *46*(5), 921–944, doi:10.1093/petrology/egi005.

Plank, T., and C. H. Langmuir (1988), An evaluation of the global variations in the major element chemistry of arc basalts, *Earth Planet. Sci. Lett.*, *90*, 349–370.

Plank, T., and C. H. Langmuir (1993), Tracing trace elements from sediment input to volcanic output at subduction zones, *Nature*, *362*, 739–743.

Porrera, C., J. Selverstone, and K. Samuels (2006), Pyroxenite xenoliths from the Rio Puerco volcanic field, New Mexico: Melt metasomatism at the margin of the Rio Grande rift, *Geosphere*, *2*(7), 333–351, doi:10.1130/GES00058.1.

Putirka, K. D. (2005), Mantle potential temperatures at Hawaii, Iceland, and the mid-ocean ridge system, as inferred from olivine phenocrysts: Evidence for thermally driven mantle plumes, *Geochem. Geophys. Geosyst.*, *6*, Q05L08, doi:10.1029/2005GC000915.

Rapp, R. P., and E. B. Watson (1995), Dehydration melting of metabasalt at 8–32 kbar: Implications for continental growth and crust-mantle recycling, *J. Petrol.*, *36*(4), 891–931.

Rapp, R. P., N. Shimizu, M. D. Norman, and G. S. Applegate (1999), Reaction between slab-derived melts and peridotite in the mantle wedge: Experimental constraints at 3.8 GPa, *Chem. Geol.*, *160*, 335–356.

Roberts, S. J., and J. Ruiz (1989), Geochemistry of exposed granulite facies terrains and lower crustal xenoliths in Mexico, *J. Geophys. Res.*, *94*(B6), 7961–7974.

Robin, C., and C. Boudal (1987), A gigantic Bezymianny-type event at the beginning of modern Volcan Popocatepetl, *J. Volcanol. Geotherm. Res.*, *31*, 115–130.

Roeder, P. E., and R. F. Emslie (1970), Olivine-liquid equilibrium, *Contrib. Mineral. Petrol.*, *29*, 275–289.

Rudnick, R. (1995), Making continental crust, *Nature*, *378*, 571–578.

Rudnick, R., and S. Gao (2002), Composition of the continental crust, in *Treatise on Geochemistry*, vol. 3, *The Crust*, edited by R. L. Rudnick, pp. 1–64, Elsevier, New York.

Ruiz, J., P. J. Patchett, and F. Ortega-Gutierrez (1988a), Proterozoic and Phanerozoic basement terranes of Mexico from Nd isotopic studies, *Geol. Soc. Am. Bull.*, *100*, 274–281.

Ruiz, J., J. Patchett, and R. J. Arculus (1988b), Nd-Sr isotope composition of lower crustal xenoliths—Evidence for the origin of mid-tertiary felsic volcanics in Mexico, *Contrib. Mineral. Petrol.*, *99*, 36–43.

Salters, V. J. M., and J. Longhi (1999), Trace element partitioning during initial stages of melting beneath mid-ocean ridges, *Earth Planet. Sci. Lett.*, *166*, 15–30.

Schaaf, P., W. Heinrich, and T. Besch (1994), Composition and Sm-Nd isotopic data of the lower crust beneath San Luis Potosi, central Mexico: Evidence from a granulite-facies xenolith suite, *Chem. Geol.*, *118*, 63–84.

Schaaf, P., J. Stimac, C. Siebe, and J. L. Macias (2005), Geochemical evidence for mantle origin and crustal processes in volcanic rocks from Popocatepetl and surrounding monogenetic volcanoes, central Mexico, *J. Petrol.*, *46*(6), 1243–1282.

Seitz, H. M., R. Altherr, and T. Ludwig (1999), Partitioning of trace elements between orthopyroxene and clinopyroxene in peridotite and websteritic xenoliths: New empirical geothermometers, *Geochim. Cosmochim. Acta*, *63*, 3967–3982.

Shaw, D. M. (1970), Trace element fractionation during anatexis, *Geochim. Cosmochim. Acta*, *34*, 237–243.

Siebe, C., V. Rodriguez-Lara, P. Schaaf, and M. Abrams (2004a), Geochemistry, Sr-Nd isotope composition, and tectonic setting of Holocene Pelado, Guespalapa and Chichinautzin scoria cones, south of Mexico City, *J. Volcanol. Geotherm. Res.*, *130*, 197–226.

Siebe, C., V. Rodriguez-Lara, P. Schaaf, and M. Abrams (2004b), Radiocarbon ages of Holocene Pelado, Guespalapa, and Chichinautzin scoria cones, south of Mexico City: Implications for archeology and future hazards, *Bull. Volcanol.*, *66*, 203–225, doi:10.1007/s00445-003-0304-z.

Siebe, C., L. Arana-Salinas, and M. Abrams (2005), Geology and radiocarbon ages of Tlaloc, Tlacotenco, Cuauhtzin, Hijo del Cuauhtzin, Teuhtli, and Ocusacayo monogenetic volcanoes in the central part of the Sierra Chichinautzin, Mexico, *J. Volcanol. Geotherm. Res.*, *141*, 225–243.

Skulski, T., W. Minarik, and B. E. Watson (1994), High-pressure experimental trace-element partitioning between clinopyroxene and basaltic melts, *Chem. Geol.*, *117*, 127–147.

Sobolev, A. V., A. W. Hofmann, V. S. Sobolev, and I. K. Nikogosian (2005), An olivine-free mantle source of Hawaiian shield basalts, *Nature*, *434*, 590–597.

Sobolev, A. V., A. W. Hofmann, D. Kuzmin, and D. Yaxley (2006), Recycled crust in the source of mantle-derived melt: How much?, paper presented a Fifth GERM Workshop, Lamont-Doherty Earth Obs., The Earth Inst. at Columbia Univ., New York.

Sobolev, A. V., et al. (2007), The amount of recycled crust in sources of mantle-derived melts, *Science*, *316*, 412–417, doi:10.1126/science.1138113.

Stolper, E., and S. Newman (1994), The role of water in the petrogenesis of Mariana trough magmas, *Earth Planet. Sci. Lett.*, *121*, 293–325.

Straub, S. M., and A. L. Martin-Del Pozzo (2001), The significance of phenocryst diversity in tephra from recent eruptions at Popocatepetl volcano (central Mexico), *Contrib. Mineral. Petrol.*, *140*(4), 487–510.

Straub, S. M., A. L. Martin-Del Pozzo, C. H. Langmuir, S. L. Goldstein, and A. B. LaGatta (2004), Processes of melt formation at Volcan Chichinautzin, Sierra Chichinautzin, central Mexican Volcanic Belt, in *Neogene-Quaternary Continental Margin Volcanism—Proceedings of the GSA Penrose Conference at Metepec, Puebla, México*, edited by G. Aguirre-Díaz, J. Macías-Vázquez, and C. Siebe, pp. 72–XX, Inst. de Geol., Univ. Nac. Auton. de Mex., Metepec, Mexico.

Straub, S. M., C. H. Langmuir, A. L. Martin-Del Pozzo, A. B. LaGatta, and S. L. Goldstein (2006), Mantle origin of andesites in the central Mexican Volcanic Belt (abstract), *Geochim. Cosmochim. Acta.*, *70*, suppl. 1, A620.

Sun, S. S., and W. F. McDonough (1989), Chemical and isotopic systematics of oceanic basalts: Implications for mantle composition and processes, in *Magmatism in the Ocean Basins*, edited by A. D. Saunders and M. J. Norry, *Geol. Soc. Spec. Publ.*, *42*, 313–345.

Tamura, Y., and Y. Tatsumi (2002), Remelting of an andesitic crust as a possible origin for rhyolitic magma in oceanic arcs:

an example from the Izu-Bonin Arc, *J. Petrol.*, *43*(6), 1029–1047.

Tatsumi, Y. (2000), Continental crust formation by crustal delamination in subduction zones and complementary accumulation of the enriched mantle I component in the mantle, *Geochem. Geophys. Geosyst.*, *1*(12), doi:10.1029/2000GC000094.

Tatsumi, Y. (2001), Geochemical modeling of partial melting of subducting sediments and subsequent melt-mantle interaction: Generation of high-Mg andesites in the Setouchi volcanic belt, southwest Japan, *Geology*, *29*(4), 323–326.

Tatsumi, Y., and E. Eggins (1995), *Subduction Zone Magmatism: Frontiers in Earth Science*, 211 pp., Blackwell Sci., Cambridge, Mass.

Tatsumi, Y., et al. (2006), The petrology and geochemistry of Oto-Zan composite lava flow on Shodo-Shima Island, SW Japan: Remelting of a solidified high-Mg andesite magma, *J. Petrol.*, *47*(3), 595–629, doi:10.1093/petrology/egi087.

Toplis, M. J. (2005), The thermodynamics of iron and magnesium partitioning between olivine and liquid: Criteria for assessing and predicting equilibrium in natural and experimental systems, *Contrib. Mineral. Petrol.*, *149*, 22–39.

Villemant, B. (1988), Trace-element evolution in the Phlegrean Fields (central-Italy): Fractional crystallization and selective enrichment, *Contrib. Mineral. Petrol.*, *98*, 169.

Wallace, P. J., and I. S. E. Carmichael (1999), Quaternary volcanism near the Valley of Mexico: Implications for subduction zone magmatism and the effects of crustal thickness variations on primitive magma compositions, *Contrib. Mineral. Petrol.*, *135*, 291–314.

Wang, Z., G. A. Gaetani, and S. R. Hart (2006), Experimental study of Ni and Mn partitioning between olivine and siliceous melt: Implications for Ni-olivines in Hawaiian lavas, *Geochim. Cosmochim. Acta*, *70*, suppl. 1, A188.

Witt-Eickschen, G., and H. O'Neill (2005), The effect of temperature on the equilibrium distribution of trace elements between clinopyroxene, orthopyroxene, olivine and spinel in upper mantle peridotite, *Chem. Geol.*, *221*, 65–101.

Wörner, G., S. Moorbath, and R. S. Harmon (1992), Andean Cenozoic volcanic centers reflect basement isotopic remains, *Geology*, *20*(12), 1103–1106.

Yaxley, G. M., and D. H. Green (1998), Reactions between eclogite and peridotite: Mantle refertilisation by subduction of oceanic crust, *Schweiz. Mineral. Petrogr. Mitt.*, *78*, 243–255.